Journal of Bioenergetics and Biomembranes, Vol. 13, Nos. 5/6, 1981

A Model for the Regulation of Brain Adenylate Cyclase by Ionic Equilibria[1]

Heripsime Ohanian,[2] Kamran Borhanian,[2] Salette de Farias, and Alfred Bennun[2,3]

Received February 22, 1981; revised May 22, 1981

Abstract

Multiple-equilibrium equations were solved to investigate the individual and separate effects of Mg^{2+}, Mn^{2+}, Ca^{2+}, ATP^{4-}, and their complexes on the kinetics of brain adenylate cyclase. The effects of divalent metals and/or ATP^{4-} (in excess of their participation in complex formation) were determined and, from the corresponding apparent affinity values, the following kinetic constants were obtained: K_m(MgATP) = 1.0 mM, $K_i(ATP^{4-})$ = 0.27 mM, K_m(MnATP) = 0.07 mM, and K_i(CaATP) = 0.015 mM. MgATP, MnATP, ATP^{4-}, and CaATP were shown to compete for the active site of the enzyme. Hence, it is proposed that endogenous metabolites with a strong ligand activity for divalent metals, such as citrate and some amino acids, become integrated into a metabolite feedback control of the enzyme through the release of ATP^{4-} from MgATP. Ca^{2+} fluxes may participate in the endogenous regulation of adenylate cyclase by modifying the level of CaATP. The free divalent metals show an order of affinity $K_{0.5}(Ca^{2+})$ = 0.02 mM, $K_{0.5}(Mn^{2+})$ = 3.8 mM, $K_{0.5}(Mg^{2+})$ = 4.7 mM, and an order of activity $Mn^{2+} > Mg^{2+} > Ca^{2+}$. The data indicate that Mn^{2+} and Mg^{2+} ions may compete for a regulatory site distinct from the active site and increase V_m without changing K_m(MgATP), K_m(MnATP), or $K_i(ATP^{4-})$. The interactions of ATP^{4-} and CaATP, which act as competitive inhibitors of the reaction of the enzyme with the substrates MgATP and MnATP, and Mg^{2+} and Mn^{2+}, which act as activators of the enzyme in the absence of hormones, are shown to follow the random rapid equilibrium BiBi group-transfer mechanism of Cleland with the stipulation that neither Mg^{2+} nor Mn^{2+}, in excess of their respective participation in substrate formation, are obligatorily required for basal activity. ATP^{4-} and CaATP are involved in dead-end inhibition. For $MgCl_2$ saturation curves at constant total ATP concentration, the computer-generated curves based on the RARE BiBi model predict a change in the Hill cooperativity h from a basal

[1]Abbreviations used: Me, divalent metal; Me_T (Mg_T or Mn_T), total Me (Me^{2+} and its complexes); ATP_T, total ATP (ATP^{4-} and its complexes).

[2]Department of Zoology and Physiology, Rutgers, The State University, Newark, New Jersey 07102.

[3]Address correspondence to A. Bennun, Department of Zoology and Physiology, NCAS, Rutgers University, Newark, New Jersey 07102.

0145-479X/81/1200-0317$03.00/0

value of 2.6, when Mg^{2+} is not obligatorily required, to 4.0 when the addition of hormones or neurotransmitters induces an obligatory requirement for Mg^{2+}.

Key Words: Kinetic models; adenylate cyclase; metal regulation; brain function; ionic equilibria; metabolic controls; calcium regulation; magnesium regulation; manganese regulation; nucleotide regulation.

Introduction

Adenylate cyclase [E.C. 4.6.1.1; ATP pyrophosphate-lyase (cyclizing)] was first studied by Rall and Sutherland (1958). Sutherland *et al.* (1962) were the first to establish that adenylate cyclase has an absolute requirement for Mg^{2+}. Subsequently, Birnbaumer *et al.* (1969) in fat cells and Drummond *et al.* (1971, 1976) in cardiac tissue established that MgATP is the true substrate for the enzyme and that free ATP is an inhibitor. These workers concluded that Mg^{2+} interacts with the enzyme at a cation binding site other than the catalytic site to activate the enzyme. The binding of Mg^{2+} to a separate binding site was reported to increase the reactivity of the catalytic site for the substate (Severson *et al.*, 1972). Subsequent proposals were advanced by De Haen (1974) that uncomplexed ATP, and by Rodbell *et al.* (1975) that $HATP^{3-}$, could function as potent inhibitors of fat cell and ventricular adenylate cyclase, and that a regulatory cation binding site was not necessary. Garbers and Johnson (1975), however, argued in favor of a separate cation binding site. The divalent cation requirement of most adenylate cyclases can be satisfied by Mn^{2+} as well as Mg^{2+} (Perkins, 1973; Johnson and Sutherland 1973). At optimal concentration of cations, adenylate cyclase activity is greater when measured with Mn^{2+} than with Mg^{2+} (Birnbaumer *et al.*, 1969; Drummond *et al.*, 1971; Johnson and Sutherland, 1973; Walton *et al.*, 1976; Hanski *et al.*, 1977). Using turkey erythrocyte ghosts, Steer and Levitzki (1975) demonstrated that Mn^{2+} substitutes for Mg^{2+} as the enzyme activator as well as forming the substrate MnATP. These investigators further suggested that Ca^{2+} has a binding site distinct from Mg^{2+} and, therefore, does not compete for the same site and that Ca^{2+} and not CaATP functions as the negative allosteric effector, inhibiting the enzyme by decreasing catalytic efficiency. Furthermore, Londos and Preston (1977) have shown that Mn^{2+} activates hepatic adenylate cyclase at very low concentrations. They suggested that Mn^{2+} may activate by binding to specific regulatory sites, an action which is independent of its ability to form a metal–substrate complex. They further proposed a similar value of V_m and K_m for both MgATP and MnATP. More recently, Neer (1979) has suggested that Mn^{2+} acts on the catalytic component of the adenylate cyclase system. Following previous procedures (Harris *et al.*, 1979; Johnson *et al.*, 1979), in the present study we solve multiple-equilibrium equations to define the

specific effect of the relevant range of concentrations of only one of the substrates, activators, or inhibitors on the kinetics of the enzyme. Thus, the kinetic constant for ADP^{4-}, MgATP, MnATP, CaATP, Mg^{2+}, Mn^{2+}, and Ca^{2+} can be evaluated independently and individually. The data were also used to determine whether free Mg^{2+} acts as an obligatory activator that controls basal activity (Garbers *et al.*, 1975; Johnson *et al.*, 1979; Rodan *et al.*, 1980a), or in a more restricted role as a nonrequired activator of the enzyme. The data obtained were then used to develop a kinetic model subject to theoretical versus experimental analysis.

Materials

Rats were obtained from Camm Research Institute (Wayne, New Jersey). The chemicals were purchased from the following sources: ATP (disodium salt) from P-L Biochemicals, Inc. (Milwaukee, Wisconsin(; norepinephrine-HCl and 3′,5′ cyclic AMP (cyclic AMP) from Sigma Chemical Co. (St. Louis, Missouri); bovine serum albumin (fraction V powder) from Pentex (Kankakee, Illinois); Tris and Tricine from General Biochemicals (Chagrin Falls, Ohio); Cyclic [^{3}H] AMP (uniformly labeled, ammonium salt) and theophylline from Schwartz Mann (Orangeburg, New York); Bray's solution (LSC cocktail *p*-dioxane based) from J. T. Backer Chemical Co. (Phillisburg, New Jersey); $CaCl_2$ (Tetrahydrate, ultrapure, optronic grade) from Alfa Inorganics (Beverly, Massachusetts); $MgCl_2$ (Hexahydrate, ultrapure, JMC high-purity grade) from Johnson Matthey Chemicals (74 Hatton Garden, London, E.C. 1, England). The latter salts as well as all other chemicals used were of reagent grade with the lowest metal contaminations commercially available. Millipore filters (0.45 μm, type HA) were obtained from Millipore Co. (Bedford, Massachusetts).

Methods

Membrane Preparation

Female Sprague-Dawley rats weighing 210–300 g were ovariectomized to decrease interference by estrus cycles (Ohanian *et al.*, 1978). They were stunned and decapitated at 4°C two weeks after surgery. The brains were immediately dissected in the cold (4°C) to isolate three areas (hypothalamus, cortex, and striatum) using the procedure of Glowinski and Iverson (1966). The cortex, striatum, and hypothalamus from groups of 10 to 15 animals were separately collected in 20 ml of ice-cold 2 mM Tris-HCl containing 10 mM

NaCl, 10 mM KCl, and 5 μM EDTA, buffer at pH 7.4, and rinsed twice with an equal volume of the same solution. The total wet weight of each pool of tissue was determined and then separately homogenized in the collecting buffer (15 ml/g wet weight of tissue) by using a motor-driven (Inframo, Wayne, New Jersey) Teflon homogenizer at 400 rpm for 2 min. Each homogenate was centrifuged at 4°C and 6000 g_{av} in an RCA Sorvall, head SS-34, for 20 min. The resulting supernatant was discarded and the pellet was washed and resuspended in an equal volume of the same buffer and centrifuged again once. The pellet was resuspended as before and 1-ml aliquots were distributed into separate vials and stored at −70°C. The preparation stored in this way was stable for at least 6 months. Protein concentration for each particle suspension was determined by the method of Lowry (Lowry *et al.*, 1951) using bovine serum albumin as the standard. Particle suspensions and reaction mixtures were tested with a calcium ion electrode for Ca^{2+} contamination with negative results.

Assay of Adenylate Cyclase Activity

The reaction was started by the addition of a recently defrosted adenylate cyclase particulate preparation (1.7–6 μg protein/assay) to a standard reaction mixture containing 20 mM Tris-HCl buffer (pH 7.4), 5 mM theophylline, ATP, $MgCl_2$, and the other additions indicated in the legends. All the additions were previously adjusted with 2 mM Tris to a final pH value of 7.4. After incubating in a shaking bath at 37°C for 15 min the reaction was terminated by heating in a boiling water bath for 5 min. Time-dependence studies using the particulate preparation showed linear responses for no less than 30 min even at the higher particle and lower substrate concentrations used for the experiments reported in the Figs 1–13. Moreover, as has been previously reported (Brydon-Golz *et al.*, 1977), the preparation from brain shows an ATPase activity of only 0.1 nmol $P_i/h/\mu g$ protein in the assay conditions used. Accordingly, since the ATP-regenerating system included during previous studies (Harris *et al.*, 1979) does not change the time course of the reaction rates, it was decided to exclude it from the assay mixture. Cyclic AMP formed by adenylate cyclase activity was measured by the Gilman method (Gilman, 1970) modified to follow the saturation assay procedure of Brown *et al.* (1972) according to previously published specifications (Harris *et al.*, 1979), but with cyclic [^{3}H]AMP increased to 20,000 c.p.m./assay. Results were calculated according to the fractional relationship $C - b/T - b$, where C represents c.p.m. obtained for the assay of the enzyme activity, T is c.p.m. for total binding (zero-time blanks), and b is the radioactivity retained in the millipore filters (moisture blanks). Curves plotted as percent total binding ($C - b/T - b$) versus log cyclic AMP (cold) show a linear response since interferences in the assays by a high concentration of

ATP or other reagents have already been discounted (Harris *et al.*, 1979). Routinely, whenever the assays yielded a percent total binding lower than 10% or higher than 85%, they were repeated while adjusting the volume of the samples to obtain values within the indicated limits. Results are expressed as nanomoles cyclic AMP formed per hour per milligram of protein, and they represent mean values of triplicates or more. The calculated S.E.M. did not exceed the value of the mean by more than 6%.

Association Constants Used for Solution of Multiple-Equilibrium Equations

The values assigned to the association constants were obtained from Taqui-Khan and Martell (1962, 1966) as follows:

$$[HATP^{3-}] = ([H^+]/K_a)[ATP^{4-}];\ K_a(ATP^{4-}) = 10^{-6.52}(M) \quad (1A)$$

$$[MgHATP^{1-}] = K_1[Mg^{2+}][HATP^{3-}];\ K_1(Mg^{2+}) = 10^{2.29}(M^{-1}) \quad (2A)$$

$$[MgATP^{2-}] = K_2[Mg^{2+}][ATP^{4-}];\ K_2(Mg^{2+}) = 10^{4.28}(M^{-1}) \quad (3A)$$

$$[MnHATP^{1-}] = K_{11}[Mn^{2+}][HATP^{3-}];\ K_{11}(Mn^{2+}) = 10^{2.3}(M^{-1}) \quad (4A)$$

$$[MnATP^{2-}] = K_{12}[Mn^{2+}][ATP^{4-}];\ K_{12}(Mn^{2+}) = 10^{4.63}(M^{-1}) \quad (5A)$$

$$[CaHATP^{1-}] = K_{21}[Ca^{2+}][HATP^{3-}];\ K_{21}(Ca^{2+}) = 10^{2.13}(M^{-1}) \quad (6A)$$

$$[CaATP^{2-}] = K_{22}[Ca^{2+}][ATP^{4-}];\ K_{22}(Ca^{2+}) = 10^{3.94}(M^{-1}) \quad (7A)$$

$$[MgTri] = K_m[Mg^{2+}][Tri];\ K_m(Mg^{2+}) = 10^{1.2}(M^{-1}) \quad (8A)$$

$$[MnTri] = K_{1m}[Mn^{2+}][Tri];\ K_{1m}(Mn^{2+}) = 10^{2.7}(M^{-1}) \quad (9A)$$

$$[CaTri] = K_{2m}[Ca^{2+}][Tri];\ K_{2m}(Ca^{2+}) = 10^{2.4}(M^{-1}) \quad (10A)$$

The expressions below represent the total concentration of the respective metal or ligand present in various forms in a mixture, and therefore $[Mg_T]$, $[Mn_T]$, $[Ca_T]$, and $[ATP_T][Tri_T]$ are known quantities.

$$Mg_T = [Mg^{2+}] + [MgHATP^{1-}] + [MgATP^{2-}] + [MgTri] \quad (11A)$$

$$Mn_T = [Mn^{2+}] + [MnHATP^{1-}] + [MnATP^{2-}] + [MnTri] \quad (12A)$$

$$Ca_T = [Ca^{2+}] + [CaHATP^{1-}] + [CaATP^{2-}] + [CaTri] \quad (13A)$$

$$ATP_T = [ATP^{4-}] + [HATP^{3-}] + [MgHATP^{1-}] + [MgATP^{2-}] + [CaHATP^{1-}] + [CaATP^{2-}] + [MnHATP^{2-}] + [MnHATP^{1-}] \quad (14A)$$

$$Tri_T = [Tri] + [MgTri] + [MnTri] + [CaTri] \quad (15A)$$

Using the above expressions, we obtain the following equations:

$$[ATP^{4-}] = ATP_T/1 + (K_2 + WK_1)[Mg^{2+}] + (K_{12} + WK_{11})[Mn^{2+}] + (K_{22} + WK_{21})[Ca^{2+}] + W \quad (16A)$$

$$[Tri] = Tri_T/(1 + K_m[Mg^{2+}] + K_{1m}[Mn^{2+}] + K_{2m}[Ca^{2+}]) \quad (17A)$$

$$[Mg^{2+}] = Mg_T/1 + (K_2 + WK_1)[ATP^{4-}] + K_m[Tri] \quad (18A)$$

$$[Mn^{2+}] = Mn_T/1 + (K_{12} + WK_{11})[ATP^{4-}] + K_{1m}[Tri] \quad (19A)$$

$$[Ca^{2+}] = Ca_T/1 + (K_{22} + WK_{21})[ATP^{4-}] + K_{2m}[Tri] \quad (20A)$$

where the term $W = [H^+]/K_a$, and if any of the three metals or tricine (Tri) were not used, the total concentration was simply taken as equal to zero when calculating the data presented here. Equations (16A)–(20A) were derived and used to calculate the concentrations of the uncomplexed forms ATP^{4-}, tricine, Mg^{2+}, Mn^{2+}, and Ca^{2+} with an iterative Fortran program which was initiated by an estimation of the free concentration at 10% of the total concentration of added metal, then recalculation of a new concentration using Eqs. (16A)–(20A) repeatedly until a precision of 0.01% was attained. The use of an Orion Research Inc. (Cambridge, Massachusetts) calcium ion electrode model 93-20 and single-junction reference electrode model 90-01 provided a direct determination of the concentration of Ca^{2+}, which was checked for consistency with the value obtained through the computer program. These values were then substituted into expressions (1A)–(15A), and the concentrations of metal–ligand complexes in the presence of buffer were calculated. At pH 7.4, the concentrations of the protonated forms of uncomplexed ($HATP^{3-}$) and complexed ATP ($MeHATP^{1-}$) were very low and were, therefore, not considered when plotting results. The equilibrium concentrations used for plotting the figures are tabulated in Appendixes A–D using $MgCl_2$ as an independent variable. Hill plots (Hill, 1913) were always linear; thus, only the ones corresponding to Figs. 7 and 9 are reported, but the values of the Hill coefficients h are included in Table I. The kinetic constants $K_{m\,app}$ and $K_{i\,app}$ were graphically obtained from Lineweaver–Burk plots (Line-

Table I. Kinetic Values from Hill and Lineweaver–Burk Plots for the Kinetic Interactions of Divalent Metal–ATP Complexes, Divalent Metal Ions, and Free ATP (ATP^{4-})

Kinetic constant					
Substrate	Modulators	K_m (mM)	$K_{m\,app}$ (mM)	h	K_i (mM)
MnATP	—	0.065	0.075	0.8	—
MnATP	ATP^{4-}	—	1.5	—	0.25
MgATP	—	1.05	2.0	1.1	—
MgATP	+2.26 mM ATP^{4-}	—	10.0	1.49	0.27
MgATP	+0.5 mM CaATP	—	20.0	0.9	0.06
MgATP	+2.2 mM Mg^{2+}	—	1.43	1.1	—
MgATP	+30.0 mM Mg^{2+}	—	1.1	0.98	—

Table II. Thermodynamic Constants Obtained from Figs. 2, 6, 7, and 9 for the Indicated E Complexes[a]

Enzyme complex	K_d[b] (mM)	K_m (mM)	K_i (mM)	$K_f \times 10^4$ (M^{-1})	$-\Delta G°$ (kcal)
E-MnATP	—	0.07		1.43	5.6
E-MgATP	—	1.0		0.10	4.1
E-CaATP	—	—	0.015	6.67	6.5
E-ATP^{4-}	—	—	0.27	0.37	4.8
E-Ca	0.02	—	—	5.0	6.4
E-Mg	4.7	—	—	0.021	3.2
E-Mn	3.8	—	—	0.026	3.3

[a] K_d, dissociation constant; K_f, formation constant for enzyme complexes; $\Delta G°$, Gibbs free energy.

[b] Taqui-Khan provided K_d values that change by only 9% by changing ionic strength no more than 100%. Since for all experiments these limits were not exceeded, the values of K_d were only subject to considerably lower deviations.

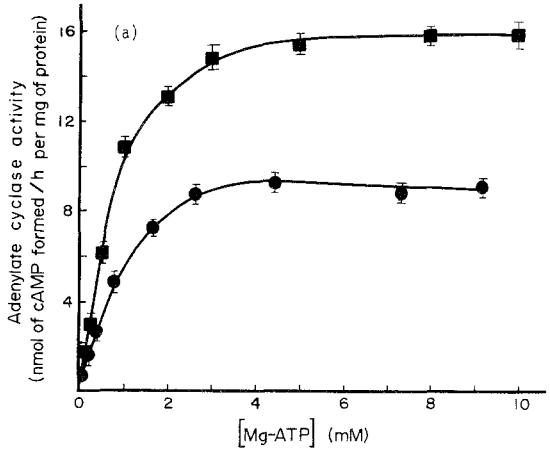

Fig. 1a. Effect of a saturating concentration of ionic magnesium on substrate saturation of corpus striatum adenylate cyclase. Portions of an adenylate cyclase particulate preparation containing 2.54 μg of protein were incubated at 37°C for 15 min in a final 0.5 ml volume of a reaction mixture containing 20 mM Tris-HCl buffer, pH 7.4, and 5 mM theophylline with increasing concentrations (0–10 mM) of MgATP adjusted to pH 7.4; ●, basal; ■, +30 mM $MgCl_2$. The incubation was terminated as described in Methods; zero-time blanks were prepared, and the cyclic AMP formed was assayed by the procedure described in Methods. Procedural steps were followed similarly for all subsequent experiments, the legends to the other figures indicating only the modifications introduced into the reaction mixtures.

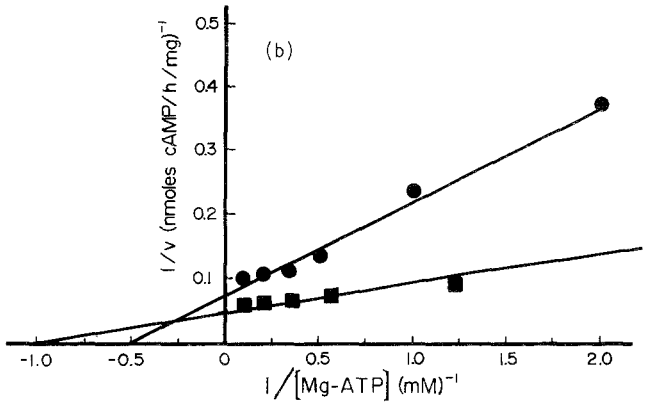

Fig. 1b. Lineweaver–Burk plot. The same symbols were used when replotting data from part a into parts b and c of figures. The plotted ionic equilibrium concentrations of divalent metal complexes are tabulated for Fig. 1a and its corresponding plots in Appendix A. The legends for subsequent figures indicate their corresponding appendixes and the tables for the obtained kinetic constants, except when these constants were included in Table I.

weaver and Burk, 1934) and are reported in Table I. ATP^{4-}-independent and free divalent metal-independent values of K_m for the substrates MgATP and MnATP were then calculated as described in Results and used to obtain the values of the other kinetic constants (Table I). Linear regression analysis was applied to check for consistency and to calculate the constants (Table II) used to examine various kinetic models.

Results

Experimental conditions were designed to meet the criteria delineated by De Haen (1974) for proper kinetic analysis based on the work of Weber (1965) and Deranleau (1969). The data in Fig. 1a show the effect on the enzyme activity of a saturating concentration of $MgCl_2$ as a function of the equilibrium concentrations of MgATP (Appendix A). The equilibrium concentrations of MgATP are higher for 30 mM excess $MgCl_2$ than for the basal curve. The plotting (Fig. 1a) according to the calculated substrate concentrations (Appendix A) excludes the effect of $MgCl_2$-dependent changes on MgATP concentration affecting the enzyme activity. Accordingly, it is possible to examine the specific response of the enzyme to an increase in Mg^{2+} from 0.4 ± 0.35 mM to 30 ± 0.1 mM (Appendix A). The Lineweaver–Burk plot (Fig. 1b) shows that the addition of 30 mM $MgCl_2$ in excess of added MgATP results in an increase in V_m from 14.7 to 22.7

nmol/h/mg with a concomitant decrease in the observed $K_{m\,app}$ from 2 mM to 1.1 mM (Table I). This increase in the V_m may be attributed to either positive allosteric modulation by Mg^{2+} or the removal of an inhibitor ATP^{4-} (Appendix A). Accordingly, further studies were required to differentiate between these two possibilities (Fig. 3). A Hill plot (Hill, 1913) of the data in Fig. 1a yields, for basal activity, an h coefficient of 1.1 which is not significantly changed in the presence of 30 mM $MgCl_2$ (Table I). This indicates that striatal adenylate cylase either has a single (independent) active site or, if there is more than one, excess Mg^{2+} does not appear to control their cooperativity in the absence of a neurotransmitter.

The experimental conditions described in the legends to Fig. 2a were obtained by adding 2.5 mM ATP in excess of the indicated substrate concentrations. The ranges of equilibrium concentrations for the basal condition were the same as those reported in the results for Fig. 1a (Appendix A, without excess $MgCl_2$). The corresponding ranges of equilibrium concentrations for the curve with 2.26 ± 0.06 mM ATP^{4-} (Appendix B) were as follows: 0.24 to 8.9 mM MgATP and 0.006 to 0.2 mM Mg^{2+} with a concentration ratio $[MgATP]/[Mg^{2+}]$ of 43 ± 1. Therefore, a constant concentration of free ATP^{4-} was maintained while allowing the concentration of MgATP to increase at a constant ratio with the increase in Mg^{2+} concentration. Figure 2a shows a marked decrease of the basal activity in the presence of excess 2.26 mM free ATP^{4-}. The concentration of Mg^{2+}, at 8.9 mM MgATP, decreases from 0.7 mM Mg^{2+} in the control (Appendix A) to 0.2 mM Mg^{2+} in the presence of excess free ATP^{4-} (Appendix B). Thus, at 8.9 mM MgATP, the addition of excess ATP^{4-} decreases the enzyme activity by only 17% when compared to that of the control, while the concentration of Mg^{2+} is reduced by more than three times. Hence, at the higher MgATP concentration the activity shown by the inhibited curve approaches the basal values, overcoming not only the inhibitory effect of ATP^{4-} but also the relatively small decrease in activity due to the decrease in Mg^{2+} concentration. The activating function of Mg^{2+} can only be shown (Fig. 1a and Appendix A) at concentrations which significantly exceed those present in excess ATP^{4-} (Fig. 2a and Appendix B). Thus, although the results shown in Fig. 2a appear to contradict the proposition that the basal reaction mechanism has an absolute requirement for Mg^{2+} (Garbers and Johnson, 1975; Johnson *et al.*, 1979; Rodan *et al.*, 1980a), they do not exclude a structural requirement for Mg^{2+} within the enzyme–membrane system (Bennun and Racker, 1969; Bennun, 1974, 1975). The former proposition would require a strict interdependence between the saturation effects of both MgATP and Mg^{2+}. This relationship is not observed in Fig. 2a since, in the excess ATP^{4-} curve, the MgATP-dependent saturation increases the reaction rate to approach V_m of the control even though the putative Mg^{2+}-dependent

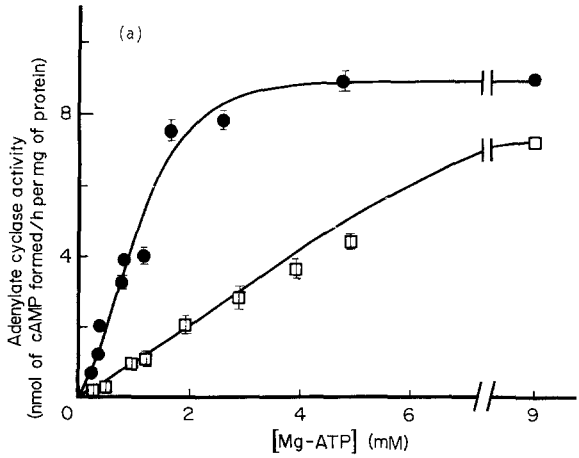

Fig. 2a. Effect of ATP^{4-} on the substrate saturation curve of corpus striatum adenylate cyclase. Portions of an adenylate cyclase particulate preparation containing 2.5 μg of protein were incubated as described in the legend to Fig. 1a; ●, basal; □, +2.5 mM added ATP. The ranges of the ionic equilibrium concentration are tabulated in Appendix A (●), and Appendix B (□).

requirement decreases with regard to that of the control, as shown when comparing Appendix A with B. The Lineweaver–Burk plot (Fig. 2b) shows that V_m is not altered by the addition of the inhibitor ATP^{4-}, whereas the observed $K_{m\,app}$ increases from 2 mM to 10 mM MgATP (Table I). Therefore, ATP^{4-} exhibits classical competitive inhibition of adenylate cyclase activity. The $K_i(ATP^{4-})$ was calculated according to the simple competitive inhibition

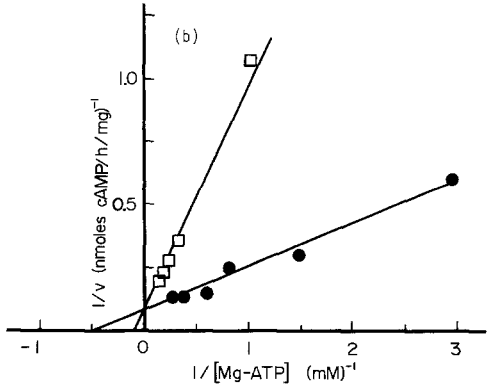

Fig. 2b. Lineweaver–Burke plot.

model for which the following rate expression (De Haen, 1974) can be written:

$$\frac{1}{v} = \frac{K_m}{V_m}\left(1 + \frac{I}{K_i}\right)\frac{1}{S} + \frac{1}{V_m} \tag{1B}$$

where $K_{m\,\mathrm{app}} = K_m(1 + I/K_i) = 10$ mM, $I = [ATP^{4-}]$, and $S = [MgATP]$. The K_m for substrate must be known in order to calculate K_i. Thus, the graphical value of K_m of 2 mM MgATP for the basal substrate saturation curve has to be corrected since it is also a $K_{m\,\mathrm{app}}$ because the concentration of ATP^{4-} increases along with that of the substrate MgATP (Appendix A). The following expression is a good approximation of the relationship of ATP^{4-} to MgATP concentration in the case of the basal curve:

$$[ATP^{4-}] = \frac{[MgHATP]^{1/2}}{K_{eq}^{1/2}} \quad \text{where} \quad K_{eq} = \frac{[MgATP]}{[Mg^{2+}][ATP^{4-}]} \tag{2B}$$

Using Eq. (2B), we can modify the rate expression for competitive inhibition [Eq. (1B)] to account for the ATP^{4-}-dependent inhibition that affects the basal substrate saturation curve [Eq. (3B)]:

$$\frac{1}{v} = \frac{K_m}{V_m}\left[1 + \frac{(S/K_{eq})^{1/2}}{K_i}\right]\frac{1}{S} + \frac{1}{V_m} \tag{3B}$$

where

$$S_{(K_{m\,\mathrm{app}})} = K_m\left\{1 + \frac{[S_{(K_{m\,\mathrm{app}})}/K_{eq}]^{1/2}}{K_i}\right\} = 2.0\ \mathrm{mM} \tag{4B}$$

Equations (1B) and (4B) are double simultaneous equations with two unknowns K_m and K_i resolved as 1.0 mM MgATP for K_m and 0.27 mM ATP^{4-} for $K_i(ATP^{4-})$ (Table II). The relationship between the values of K_m and $K_i(ATP^{4-})$ indicate that the enzyme has a greater affinity for the inhibitor ATP^{4-} than for its substrate. Accordingly, the effect of ATP^{4-} is only that of a competitive inhibitor of the substrate at the active site. Therefore, because ATP^{4-} does not exhibit an allosteric effect, the increase in V_m associated with the addition of 30 mM $MgCl_2$ to the substrate saturation curve (Fig. 1b) cannot be attributed to the $MgCl_2$-dependent reduction in the concentration of ATP^{4-} (Appendix A). The latter would have only changed $K_{m\,\mathrm{app}}$ but not V_{max}. The experimental conditions reported in the legend to Fig. 3a were selected to examine the regulatory mechanism by which Mg^{2+} interacts with the adenylate cyclase. Appropriate concentrations of both $MgCl_2$ and disodium ATP, at pH 7.4, were included in the reaction mixture to maintain in one of the curves a constant concentration of 2.17 ± 0.09 mM Mg^{2+} at a constant $[MgATP]/[ATP^{4-}]$ ratio of 41.4 ± 1.6 (Appendix C). The adjusted reaction mixtures for the basal curve allow the former ratio

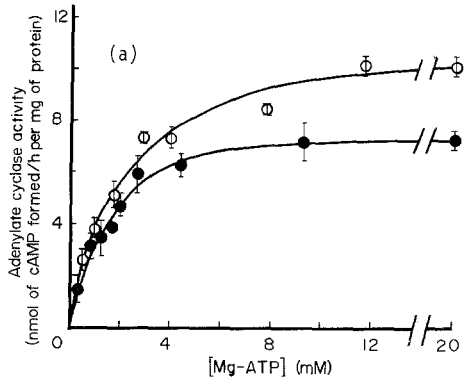

Fig. 3a. Effect of ionic magnesium at a constant $MgATP/ATP^{4-}$ concentration ratio on the substrate saturation curve of corpus striatum adenylate cyclase. Portions of an adenylate cyclase particulate preparation containing 2.5 μg of protein were incubated as described in the legend to Fig. 1a except that the concentrations of $MgCl_2$ and disodium ATP were selected to maintain a constant $MgATP/ATP^{-4}$ concentration ratio (shown in Appendix C) of 41.4 ± 1.6. ●, basal; ○, +2.17 mM excess Mg^{2+}.

(Appendix A) to increase until it approaches the same value at 2.17 mM excess Mg^{2+}. Hence, the degree of inhibition of the enzyme by the competitive inhibitor ATP^{4-} becomes the same for the basal and the 2.17 mM excess Mg^{2+} curves. Thus, the only significant difference remaining between the two curves is the Mg^{2+} concentration. The Lineweaver–Burk plot (Fig. 3b) shows a noncompetitive mechanism in which there is a decrease in $K_{m\,app}$ and an increase in V_m. Hence, the resulting increase in V_m could be directly attributed to a positive modulating effect of Mg^{2+} on a regulatory site of adenylate cyclase. This interaction of Mg^{2+} with the enzyme could correspond to a magnesium–enzyme complex (Table II), show in the equilibrium equations as Mg · E. (Schemes 1–3). As a means of checking the assumptions

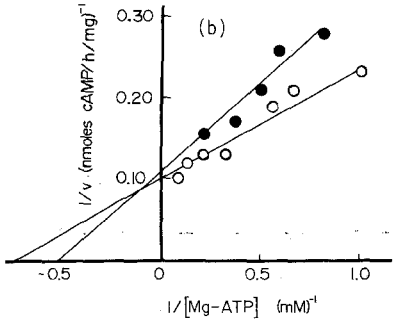

Fig. 3b. Lineweaver–Burk plot.

presented, the $K_{m\,app}$ for the 2.17 mM excess Mg^{2+} substrate saturation curve may be predicted based on Eq. (1B), the constant [MgATP]/[ATP^{4-}] ratio of 41, and the previously determined values of $K_{i(ATP^{4-})}$ and $K_{m(MgATP)}$. This can then be compared to the experimentally observed value:

$$K_{m\,app} = K_m\left(1 + \frac{[I]}{K_i}\right), \quad \text{where} \quad [I] = [ATP^{4-}] = K_{m\,app}/41 \qquad (1C)$$

Rearranging and substituting the values for K_m and K_i (Table II), we obtain

$$K_{m\,app} = \frac{K_m}{(1 - K_m/41K_i)} = 1.4 \text{ mM (1.43 observed, Table I)} \qquad (2C)$$

The proximity of the observed $K_{m\,app}$ (Table I) and the calculated one further confirm the validity of the computational approach to obtain K_m(MgATP) and K_i(ATP^{4-}) and the assumptions used in their derivation. Finally, having established that Mg^{2+} is an allosteric modulator of adenylate cyclase activity, its kinetic properties may be analyzed. As reported in Fig. 2a, 2.5 mM ATP^{4-} lowered the equilibrium concentration of Mg^{2+} from the basal range of 0.05–0.7 mM to 0.006–0.2 mM without significantly decreasing the V_m. Therefore, the above range of Mg^{2+} concentrations has no significant activating effect on adenylate cyclase. Hence, the K_d (dissociation constant of the Mg · E complex) for Mg^{2+} is relatively high, indicating low affinity of the enzyme for Mg^{2+} (Table II). Furthermore, the calculated K_m(MgATP) of 1 (Table II) is so close to the $K_{m\,app}$ of 1.1 for the substrate saturation curve in the presence of 30 mM excess Mg^{2+} (Table I) that it can safely be assumed that the activation of adenylate cyclase by Mg^{2+} is not accompanied by a change in its affinity for the substrate. Table III shows a comparison of the kinetic constants $K_{m\,app}$(MgATP) and h(MgATP) obtained for adenylate cyclase from hypothalamus, corpus striatum, and cortex. No significant difference is seen in these constants. Therefore, the regional differences in the characteristics of brain adenylate cyclase are probably not related to its responsiveness to the ionic environment. More likely, they are based on the characteristic responsiveness of adenylate cyclase to neurotransmitters. However, the apparent affinity for the substrate is about six times higher than

Table III. Values of K_m and the Apparent Hill Coefficient h for Adenylate Cyclase Obtained from Experiments Using Particulate Membrane Preparations from the Cortex, Striatum, and Hypothalamus

	$K_{m\,app}$ (mM)	h
Cortex	2.2	1.4
Striatum	2.0	1.1
Hypothalamus	2.0	1.1

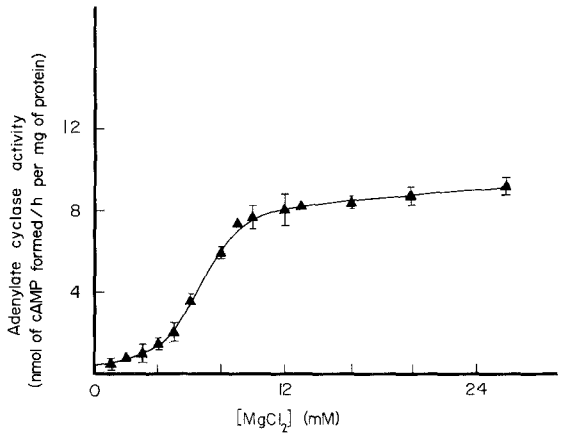

Fig. 4. Equilibrium-dependent relationships in sigmoidal response of magnesium-dependent activation of corpus striatum adenylate cyclase. Portions of an adenylate cyclase particulate preparation containing 1.76 μg of protein were incubated as described in the legend to Fig. 1a except that the experiment was modified to include a constant concentration of 5 mM total ATP (ATP_T) with increasing concentrations (0–30 mM) of $MgCl_2$.

the values reported for some other tissues (Rodan *et al.*, 1980b; Glynn *et al.*, 1979; Drummond and Duncan, 1976), but only about two times higher than for skeletal muscle (Severson *et al.*, 1972). The difference between preparative methods makes it impossible to determine whether K_m(MgATP) reflects specific adaptations to the endogenous environment of each tissue. It has been reported (Johnson and Sutherland, 1973) that EGTA, but not EDTA, releases metals tightly bound to the rat brain enzyme. Accordingly, EDTA-treated particles were used in order to examine the role of Mg^{2+} in the kinetics of the membrane-bound enzyme. Increasing amounts of $MgCl_2$ were added to a constant concentration of total ATP to examine simultaneously all

Table IV. Effect of Hormone and Calcium on Apparent Kinetic Constants of Striatal Adenylate Cyclase for Mg_T, Mg^{2+}, and ATP^{4-}

Constant determined	Basal	Norepinephrine (0.1 mM)	0.1 mM norepinephrine + 0.3 mM $CaCl_2$
$h(Mg_T)$	2.67	4.36	2.26
$S_{0.5}(Mg_T)$	8.00×10^{-3} M	8.90×10^{-3} M	9.35×10^{-3} M
$h(Mg^{2+})$	1.05	1.88	1.25
$S_{0.5}(Mg^{2+})$	4.67×10^{-3} M	4.57×10^{-3} M	4.63×10^{-3} M
$h(ATP^{4-})$	1.09	1.94	1.29
$S_{0.5}(ATP^{4-})$	0.11×10^{-3} M	0.09×10^{-3} M	0.11×10^{-3} M

of the aforementioned contributions of $MgCl_2$ to adenylate cyclase activity (Fig. 4 and Table IV). The sigmoidal response to adenylate cyclase (Fig. 4) corresponds to a Hill coefficient of 2.6. The substrate saturation experiments (Figs. 1–3) indicate the existence of only one active site with no significant change in cooperativity upon addition of excess $MgCl_2$ (Table I). However, the addition of $MgCl_2$ in this experiment is associated with a significant increase in the concentration of the substrate MgATP (from 0 to 5 mM), a decrease in the concentration of the competitive inhibitor ATP^{4-} (from 5 mM to $\simeq$0), and an increase in the concentration of the allosteric activator Mg^{2+} (from 0 to $\simeq$25 mM). Accordingly, the sigmoidal nature of this curve is due to the summation of the effects of changes in the concentrations of ATP^{4-}, Mg^{2+}, and MgATP on adenylate cyclase (Harris *et al.*, 1979). Thus, the plot of enzyme activity in the absence of neurotransmitters (Fig. 4 and Table IV) versus $MgCl_2$ concentration does not show cooperativity but only dependence on three simultaneous functions of opposite changes in the concentration of Mg^{2+} and ATP^{4-}. According to our stipulations (Scheme 3) for the rapid random equilibrium BiBi mechanism (RARE BiBi) (Cleland, 1963) three functions interrelate to yield a theoretical value of h of 2.6. These functions are (1) the decrease of the concentration of the competitive inhibitor ATP^{4-} which increases the substrate-dependent saturation of the enzyme with formation of the ternary E-MgATP complex (ES); (2) the Mg^{2+}-dependent increase in the concentration of MgATP; and (3) the Mg^{2+}-dependent increase of the quaternary Mg-E-MgATP complex (Mg · ES) having a higher V_m than the ternary complex. A preceding publication (Brydon-Golz *et al.*, 1977) reported the effect of 0.1 mM norepinephrine alone and with 0.3 mM $CaCl_2$ on $MgCl_2$ saturation curves. These were obtained in studies of the adenylate cyclase activity of EDTA-treated particles from brain corpus striatum incubated in 40 mM Tricine-Tris buffer of pH 7.4 and with constant 1 mM ATP. The kinetic constants for these studies were calculated and are reported in Table IV. These data show that, in the presence of 0.1 mM norepinephrine, the h value of the cooperativity for $MgCl_2$ (Mg_T) increases from a basal value of 2.67 to 4.36, reflecting the increases of $h(Mg^{2+})$ from 1.05 to 1.88 and $h(ATP^{4-})$ from 1.09 to 1.94. The inclusion of both norepinephrine and $CaCl_2$ reduces considerably the effect of norepinephrine alone on the values of h. The inclusion of norepinephrine and norepinephrine with $CaCl_2$ also increases the $S_{0.5}(Mg_T)$ from a basal value of 8.0 to 8.9 and 9.35 mM respectively. However, the $S_{0.5}(Mg^{2+})$ and $S_{0.5}(ATP^{4-})$ are not significantly changed from those of the basal condition (Table IV). These results indicate that norepinephrine only affects V_m and does not change the affinity of the enzyme for Mg^{2+} or for ATP^{4-}. Hence, the norepinephrine-induced increase of the value of $h(Mg_T)$ cannot be attributed to a change in the relative state of saturation of separate Mg^{2+} and MgATP sites with

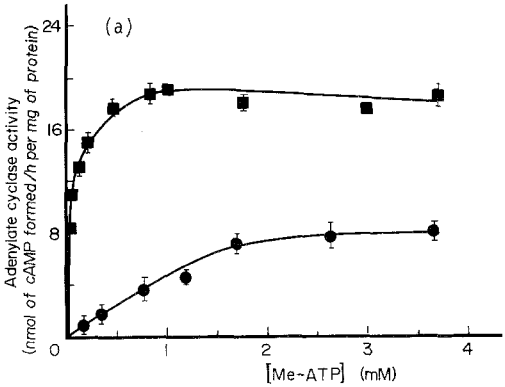

Fig. 5a. MgATP and MnATP substrate saturation curves of corpus striatum adenylate cyclase. Portions of an adenylate cyclase particulate preparation containing 6 μg of protein were incubated as described in the legend to Fig. 1a except for the modifications indicated in the plot. The plot shows activity versus equilibrium concentration of Me-ATP. ●, MgATP; ■, MnATP.

respective values of $h(Mg^{2+})$ and $h(ATP^{4-})$ or $h(MgATP)$ (Table I) close to 1. Thus, norepinephrine obviously induces cooperativity because the increase in $h(Mg^{2+})$ indicates an increase in the strength of interaction between two Mg^{2+}-requiring sites. The increase in $h(ATP^{4-})$ may only reflect the opposite change in the concentration of ATP^{4-} which simultaneously increases the state of saturation of the active site and one of the sites showing cooperativity for Mg^{2+}.

The experimental conditions described in the legend to Fig. 5a were selected to study MnATP as a substrate for adenylate cyclase and to compare its affinity with that of MgATP. Enzyme activity was plotted as a function of

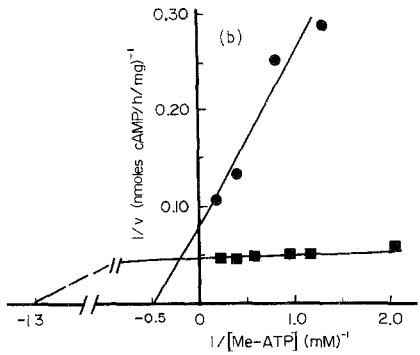

Fig. 5b. Lineweaver–Burk plot.

the equilibrium concentration of the divalent metal–ATP complex; MgATP or MnATP concentrations were calculated as described in Methods. This allowed a comparison of activity at the same concentration of MgATP or MnATP and, therefore, permitted a determination of the V_m and the K_m for each substrate with the same preparation of enzyme and relating them within the same scale of specific activity. Figure 5a shows a marked increase in adenylate cyclase activity when MnATP is used as a substrate.

The Lineweaver–Burk plot (Fig. 5b) shows that MnATP has a K_m 25 times smaller and a V_m two times greater than those observed for MgATP. The Hill plot does not show a significant difference between the values of 1.1 for h(MgATP) and 0.8 for h(MnATP) (Table I).

Figure 6a shows the effect of adding 5.5 mM ATP in excess of that in the basal curve at the indicated concentrations of MnATP. Equilibrium conditions similar to those of Fig. 2a allowed the increase of the equilibrium concentration of MnATP in the presence of negligible concentrations of Mn^{2+} ($\log K_a = 4.6$) while maintaining a constant concentration of ATP^{4-}, well above that in the basal curve. Although in the presence of excess free ATP^{4-} Fig. 6a shows a marked decrease of the basal activity of the enzyme, the inhibited curve approaches the basal at the higher MnATP concentrations.

The Lineweaver–Burk plot (Fig. 6b) shows classical competitive inhibition by ATP^{4-} on MnATP-dependent saturation of the enzyme; the V_m remains unchanged, whereas $K_{m\,app}$(MnATP) changes from 0.075 to 1.5 mM (Table I). The K_i value for ATP^{4-} was calculated based on the K_m(MnATP) and $K_{m\,app}$(MnATP with excess ATP^{4-}) using the previously presented equations for competitive inhibition. The K_i thus obtained in this experiment is 0.25 mM, essentially the same as the value determined with MgATP (0.27 mM) (Table I). Therefore, MgATP, MnATP, and ATP^{4-} bind to the same site on the enzyme. Furthermore, the presence of MnATP does not alter the affinity of the enzyme for ATP^{-4}, ruling out indirect effects of Mn^{2+} on the affinity of the enzyme for ATP^{4-}. Figure 7a shows the effect of a saturating range of $MgCl_2$ concentrations on $MnCl_2$-dependent saturation curves of the enzyme at a constant total concentration of 5 mM ATP. The basal curve of Fig. 7a shows that there is no activity at 0 mM $MgCl_2$, but with each addition of $MnCl_2$, increasing velocity is noted. Here, Mn^{2+} is complexed by ATP^{4-} to form MnATP. The latter, as shown in Fig. 5, is a substrate with high affinity for the enzyme. Therefore, the increasing activity observed at 0 mM $MgCl_2$ with each indicated addition of $MnCl_2$ is due to the formation of MnATP, decreasing ATP^{4-} and increasing Mn^{2+}, which may substitute for Mg^{2+} as an enzyme activator. The absence of included $MgCl_2$ in the basal curve results in a $MnCl_2$-dependent sigmoidal response of adenylate cyclase. This response is similar to that shown by the enzyme as a function of $MgCl_2$ saturation (Fig. 4). The inclusion of the concentration of $MgCl_2$, indicated in Fig. 7a, leads to a stimulation of the activity of the enzyme relative to that shown by the basal

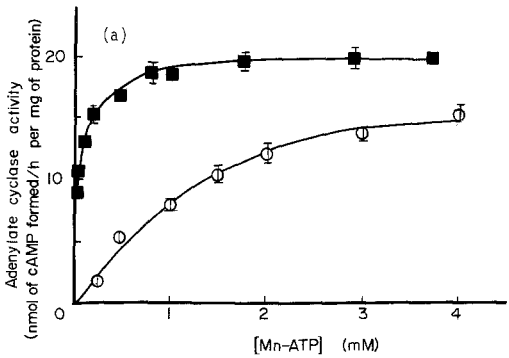

Fig. 6a. Effect of ATP^{4-} on MnATP saturation curve of corpus striatum adenylate cyclase. Portions of an adenylate cyclase particulate preparation containing 6 μg of protein were incubated as described in the legend to Fig. 1a except for use of MnATP as the substrate, plotted at equilibrium concentration. ■, basal; O, +5.5 mM ATP. As described in the legend to Fig. 2a a constant equilibrium concentration of ATP^{4-} was maintained while allowing the equilibrium concentration of MnATP to increase.

curve in the range of 0 to 4 mM $MnCl_2$. This activation is due to increasing MgATP and Mg^{2+} and decreasing ATP^{4-} concentrations. Between 4 to 6 mM $MnCl_2$, the curves show a shift from activation to inhibition of the enzyme. Above 6 mM $MnCl_2$, there is significant inhibition with each addition of $MgCl_2$. The latter effect occurs in a range where ATP^{4-} and MgATP are not capable of competing with MnATP, which is at saturating concentrations (Table I). The transition from positive to negative dependence

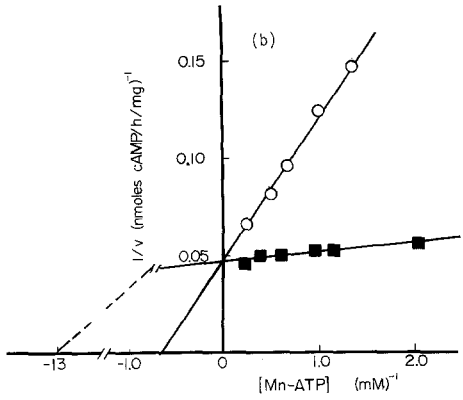

Fig. 6b. Fig. 6b. Lineweaver–Burk plot.

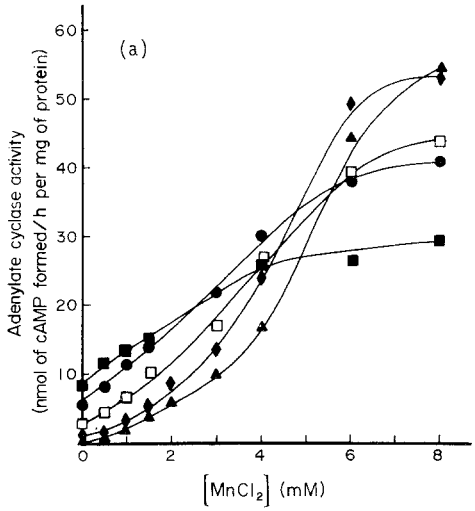

Fig. 7a. Effect of $MgCl_2$ on $MnCl_2$-dependent activation of corpus striatum adenylate cyclase at a constant ATP_T. Portions of a particulate preparation of adenylate cyclase containing 1.8 μg of protein were incubated as described in Fig. 1a except for the inclusion of 5 mM disodium ATP, pH 7.4, and 0–8 mM $MnCl_2$ in the absence (basal) and presence of the following additions: ▲, basal; ♦, +2 mM $MgCl_2$; □, +4 mM $MgCl_2$; ●, +8 mM $MgCl_2$; $MgCl_2$; ■, + 20 mM $MgCl_2$. The calculated standard deviation did not exceed 5% of the mean activity of quadruplicate assays.

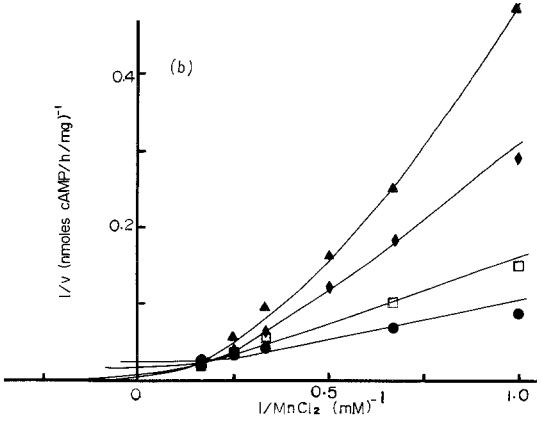

Fig. 7b. Lineweaver–Burk plot.

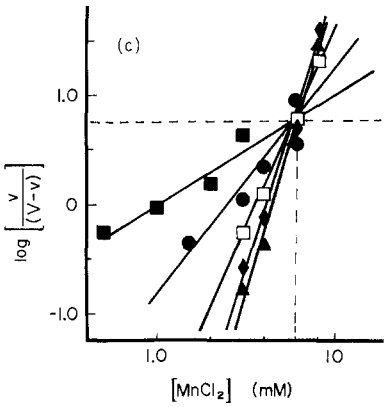

Fig. 7c. Hill plot. The values obtained for h and $S_{0.5}$ are reported in Table V.

of adenylate cyclase activity on added $MgCl_2$ is best noted at 8 mM $MnCl_2$ (Fig. 7a). Between 0–20 mM $MgCl_2$ at 8 mM $MnCl_2$ the concentrations of MnATP, MgATP, ATP^{4-}, Mn^{2+}, and Mg^{2+} (the first three are expressed as a multiple of their respective affinities) are as follows: 66- to 30-fold K_m(MnATP), 0 to 2.8-fold K_m(MgATP), 0.16- to 0.03-fold $K_i(ATP^{4-})$, 3 to 5.8 mM Mn^{2+}, and 0 to 17 mM Mg^{2+}, respectively. Clearly, there are negligible competitive effects by MgATP or ATP^{4-} on the MnATP-dependent saturation of the active site. Thus, the inhibition of adenylate cyclase activity between 0–20 mM $MgCl_2$ must be related to the interactions of Mg^{2+} and Mn^{2+} (Table V). Furthermore, the 6 and 8 mM $MnCl_2$ concentrations were the only instances where this metal was added in excess of the total ATP (5 mM). Hence, Mn^{2+} activation of adenylate cyclase is expected to be present without the additions of $MgCl_2$. Thus, the decrease in the activity of adenylate cyclase with the addition of $MgCl_2$, in the presence of 6 and 8 mM $MnCl_2$, corresponds to the displacement of a stronger Me^{2+} activator of adenylate cyclase, namely Mn^{2+}, by a weaker one, Mg^{2+}. In conclusion, Mg^{2+} and Mn^{2+} activate and compete for the same site on the enzyme.

Table V. Effect of Magnesium on Adenylate Cyclase Apparent Kinetic Constants for Manganese[a]

Constant determined	Basal	2 mM $MgCl_2$	4 mM $MgCl_2$	8 mM $MgCl_2$	20 mM $MgCl_2$
V_m[b]	57.5	56.5	44.5	43.0	26.5
$h(Mn_T)$	5.29	5.11	3.71	2.16	1.12
$S_{0.5}(Mn_T)$[c]	4.39×10^{-3} M	4.03×10^{-3} M	3.60×10^{-3} M	2.44×10^{-3} M	1.01×10^{-3} M

[a] The kinetic constants were obtained from the $MnCl_2$ saturation curve (Fig. 7a) and the corresponding Hill plot (Fig. 7c).
[b] Adenylate cyclase activity (nmol of cAMP formed per hour per milligram of protein).
[c] $S_{0.5}$ is substrate or divalent metal concentration at $0.5V_{max}$.

The Lineweaver–Burk plot (Fig. 7b) shows an intersection point at about 5.5 mM $MnCl_2$, or just above the total ATP concentration. For $MnCl_2$ concentrations below this point, additions of $MgCl_2$ lead to an increase in Me^{2+}-dependent activation, and a decrease in ATP^{4-} inhibition. Above 5.5 mM $MnCl_2$, further additions of $MgCl_2$ lead to increasing Mg^{2+} and MgATP competition with Mn^{2+} and MnATP for their respective sites, resulting in decreasing activity. Hence, the mixed competitive appearance of the plot shown in Fig. 7b can be simply explained by the competition of the dissociated and complexed forms of both divalent metals for two sites with different affinities, namely the substrate (MeATP) and Me^{2+} binding sites.

The Hill plot (Fig. 7c) shows an intersection point at 6 mM $MnCl_2$ associated with a simultaneous decrease in $S_{0.5}$ and the Hill coefficient (Table V). A perpendicular drawn from the intersection point to the ordinate intersects the axis at log $(v/(V - v) = 0.75$. This perpendicular corresponds to the expected response of adenylate cyclase at infinite concentrations of added $MgCl_2$, where all the available ATP (5 mM) would be converted to MgATP with the concentrations of MnATP reaching zero and all of the added $MnCl_2$ in the Mn^{2+} state. The value of the intercept of this line (0.75), when introduced into the Hill equation, yields a velocity equal to 85% of V_m. Similarly, the corresponding concentration of MgATP (5 mM), if substituted in the enzyme–substrate equilibrium equation $K_a = [E-MgATP]/[E][MgATP] = 1 \times 10^3\ M^{-1}$ or $1/K_m$, indicates 84% saturation of the active site. Therefore, this intersection indicates competition of MgATP with MnATP, whereas Mn^{2+} competes with Mg^{2+}, confirming the values of 1 mM for the K_m(MgATP) or $K_a = 1 \times 10^3\ M^{-1}$ (Tables I and II).

Figure 8 is a plot of experimental data obtained under the same conditions described in the legend to Fig. 7a. The plot shows the basal curves for $MgCl_2$ and $MnCl_2$ saturation of the enzyme only in the range of concentrations in excess of the added 5 mM ATP. The purpose of this plot is to demonstrate Mg^{2+} and Mn^{2+} activation of adenylate cyclase. This analysis is based on the premise that when the concentration of $MeCl_2$ equals that of total ATP (5 mM), the amount of MeATP formed is sufficient to nearly saturate the active site. Accordingly, any further increases in activity beyond this concentration of $MeCl_2$ are due to Me^{2+} activation of adenylate cyclase. This occurs only if the divalent metal is in excess of that required to form the MeATP complex (Fig. 2). Thus, by plotting the percent increase in activity beyond the 5 mM concentration of $MeCl_2$ versus the concentration of Me^{2+}, it is possible to subtract the effects expected from a decrease in ATP^{4-}, and to illustrate the kinetic similarity between the activation effects attributable directly either to Mg^{2+} or to Mn^{2+}. Figure 8 allows the computation of values of 4.7 mM $MgCl_2$ for $K_m(Mg^{2+})$ and 3.8 mM $MnCl_2$ for $K_m(Mn^{2+})$. Table II shows the corresponding dissociation constants for the E-Mg and E-Mn

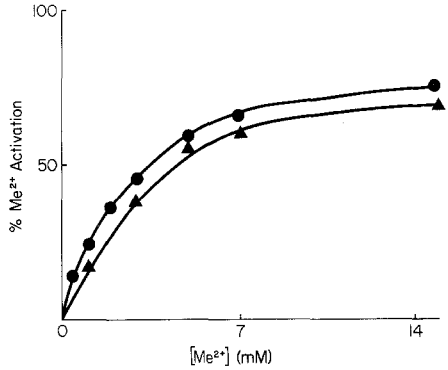

Fig. 8. Mg^{2+}- and Mn^{2+}-dependent percent activation of adenylate cyclase. Activity data for the basal curves of $MgCl_2$ and $MnCl_2$ saturation of adenylate cyclase were obtained using similar conditions as those reported in Fig. 7a and were respectively plotted as percent activation of the enzyme calculated by using the equation $[(V - v_{(5\ mM)}/(V_m - v_{(5\ mM)}] \times 100$, where $v_{(5\ mM)}$ is the velocity at 5 mM $MeCl_2$ concentration, V is the velocity at a given concentration beyond 5 mM $MeCl_2$, and V_m is the velocity at maximal Me^{2+} activation. The percent Me^{2+}-dependent activation was plotted as a function of Me^{2+} concentration; ▲, Mg^{2+}; ●, Mn^{2+}.

complexes based on the assumption that at 50% Me^{2+} activation (Fig. 8), there are equal concentrations of enzyme complexes alone and with Me^{2+} at the Me^{2+}-dependent regulatory site. Table II compares the thermodynamic quantities associated with the interaction of the enzyme with MeATP and metal ions (Taqui-Khan and Martell, 1966; Lineweaver and Burk, 1934) and shows that K_f(E-MnATP) exceeds K_f(E-MgATP). The former is therefore capable of maintaining a relatively higher value of $-\Delta G°$ for the interconversion of ES complex into EP complex, since K_f(EP) would be the same for both substrates. The greater the value of $-\Delta G$ for the steady-state ratio [ES]/[EP], the larger becomes the difference favoring the forward versus the reverse rate of interconversion ES $\rightleftharpoons$ EP. Thus, the affinity-dependent thermodynamic parameters discussed appear to have a potential to affect reaction rates. Accordingly, the higher V_m observed in the presence of MnATP (Fig. 5) may be related to a proportionally larger $-\Delta G°$ (Table II) during the turnover of the ternary complex E-MnATP. The formation constants of the quaternary complexes Me · E-MeATP [summation of K_f(E-MeATP) and K_f(E-Me), Table II] exceed those of their respective

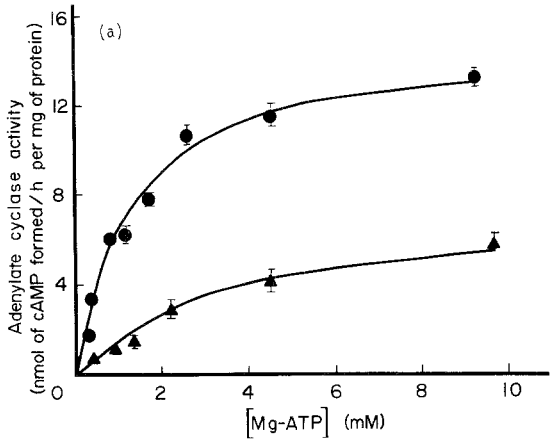

Fig. 9a. Effect of CaATP on the substrate saturation curve of hypothalamic adenylate cyclase. Portions of a particulate membrane preparation containing 3.3 μg of protein were incubated as described in the legend to Fig. 1a with increasing equimolar $MgCl_2$ and ATP (0–10 mM) concentrations (Appendix D). ●, basal; ▲, in the presence of 0.5 mM CaATP.

ternary complexes an so may explain the higher V_m values observed for the quaternary complexes.

The effect of CaATP on the substrate saturation curve (Fig. 9a) was evaluated by varying the equilibrium concentrations of MgATP from 0.41 to 9.3 mM MgATP and adding 0.5 mM CaATP to maintain its equilibrium concentration within the range of 0.33 to 0.42 mM CaATP (Appendix D). Figure 9a shows that the addition of 0.5 mM CaATP results in a significant

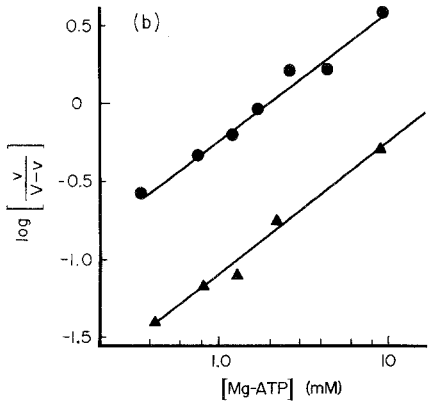

Fig. 9b. Hill plot.

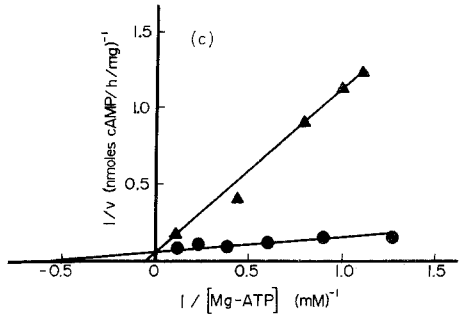

Fig. 9c. Lineweaver–Burk plot.

inhibition of the substrate saturation curve. Figure 9b shows a Hill plot of the data in Fig. 9a. The control curve shows an h value of 1.1, which was decreased by CaATP to 0.9. The Lineweaver–Burk plot (Fig. 9c) shows competitive inhibition between CaATP and substrate. CaATP increases $K_{m\,app}$ for the substrate from 2 mM to 20 mM MgATP (Table I). From the latter, a value of 0.06 mM was calculated for Mg^{2+} and ATP^{4-}-independent K_i(CaATP). The quantity K_i(CaATP) (Table I) is an apparent K_i and, therefore, further studies are necessary to compute a Ca^{2+}-independent value of K_i(CaATP) (Ohanian, Borhanian, and Bennun, unpublished). These studies show that the $CaCl_2$ saturation curves, at added 1 mM MgATP, yield a value of 0.016 mM $K_{i\,app}(Ca^{2+})$ and 0.6 apparent $h(Ca^{2+})$. The addition of several concentrations of $MgCl_2$ to the $CaCl_2$ saturation curves did not change $K_i(Ca^{2+})$ but resulted in a Mg^{2+}-dependent decrease in the negative cooperativity for Ca^{2+}. Analysis of these curves showed that the effect of equilibrium concentrations of Mg^{2+}, MgATP, and ATP^{4-} on the percentage of the relative saturation of the active site and Mg^{2+}-modulated site remained constant within the range 10^{-7} to 10^{-3} M $CaCl_2$. Accordingly, the negative cooperativity shown by the enzyme in response to $CaCl_2$ can only be explained by Ca^{2+} reducing the inhibitory effect of CaATP. The latter becomes evident when a plot of Ca^{2+} saturation curves (as a function of the expected and observed effect of CaATP) shows a weak activating effect by concentrations of Ca^{2+} within the range tabulated in Appendix D. If this effect is taken into consideration, the $CaCl_2$ saturation curves yield a value of 1 for $h(Ca^{2+})$. Hence, the inhibitory effects of Ca^{2+} may be attributed to Ca^{2+} displacing Mg^{2+} from a Mg · E-MgATP quaternary complex to form a Ca · E-MgATP quaternary complex of considerably lower activity. Accordingly, we re-evaluated the kinetic constants, and a K_d(E-Ca) of 0.02 (Table II) was obtained from $K_i(Ca^{2+})$. Similarly, after correcting for the weak activity of Ca · E-MgATP in the curve with excess 0.5 mM CaATP (Appendix D and

Fig. 9a), a Ca^{2+}-independent value of 0.015 mM K_i(CaATP) was obtained (Table II).

Synthesis of a Model and Rate Expression for the Kinetics of Adenylate Cyclase

Several mechanistic models were evaluated to determine their applicability to the kinetics of rat brain adenylate cyclase on the basis of the following stipulations: (1) One atom of divalent metal participates in the formation of substrate (MgATP or MnATP), and a second atom, Mg^{2+} or Mn^{2+} may be acting either as an obligatory activator or as a modulator to increase V_m, but without modifying the K_m(MeATP). (2) ATP^{4-} is only a competitive inhibitor. (3) Accepting the reasons delineated by De Haen (1974), we used the steady-state assumption and later evaluated it in terms of experimental evidence. (4) MeATP and ATP^{4-} represent the summation of their protonated and dissociated forms. In our experimental conditions (constant pH), the concentration ratios of both $MeHATP^{1-}$ to $MeATP^{2-}$ and $HATP^{3-}$ to ATP^{4-} are smaller than 0.1 and changed even less than 1%. Therefore, the effect of one form cannot be differentiated from the other.

The rate equation for each of the models we examined was either obtained from the literature or derived using the King–Altman technique (1956). The constants for a given rate equation were usually derived by assuming the rate equation to be correct and applying it to the Lineweaver–Burk plots of experimental points for Figs. 1 and 2, where the V_m for the basal condition was translated into 1.0. The rate equation was simplified, and individual constants were obtained. An iterative program was then used to adjust the constants using the least-squares technique to derive the best possible fit. If a constant could not be derived, an arbitrary value was assigned based on the values suggested in the literature, and then the iterative technique was applied. The initial attempt at fitting was performed using the data for the $MgCl_2$ saturation curve in Fig. 4. The latter allows for greater than 75% saturation of both substrate and Me^{2+} sites, thus fulfilling an important criterion in the analysis of kinetic data (Weber, 1965; Deranleau, 1969). The goodness of fit for the Lineweaver–Burk plot, Hill plot, and the plot of v versus $MgCl_2$ added was checked in that order. The first attempt to fit the data involved using the rate expression for the De Haen model (De Haen, 1974), Eq. (1B). Thus, in (1B) when the concentration of ATP^{4-} approaches zero (Fig. 1), the term $1 + [ATP^{4-}]/K_i$ was omitted [rate expression (1C)], and when the concentration of ATP^{4-} was held constant (Fig. 2), $K_{m\,app}$ replaced K_m [rate expression (2C)]. These rate expressions (De Haen, 1974) indicate that the Lineweaver–Burk plots for excess 30 mM Mg^{2+} (Fig. 1b) and excess 2.5 mM ATP^{4-} (Fig. 2b) in the substrate

saturation curves should approach the same V_m. Therefore, these rate expressions fail to predict the Mg^{2+}-dependent change in V_m (Fig. 1). Furthermore, an adequate fit cannot be obtained for the $MgCl_2$ saturation curve since the De Haen model predicts an $h(MgCl_2)$ value of 1.4, as compared to the experimental value of 2.6 (Fig. 4) (Harris *et al.*, 1979; Brydon-Golz *et al.*, 1977). Hence, there is a site for Mg^{2+} which was not taken into account by De Haen (1974). We then considered the Johnson and Sutherland model (Johnson and Sutherland, 1973) and its predictions that ATP^{4-} is an inhibitor, type unstated, and Mg^{2+} is required to form an active enzyme (Hammes B state) (Hammes and Rodbell, 1976). The schematic as suggested by Hammes (Hammes and Rodbell, 1976) was modified for competitive ATP inhibition. The resulting scheme corresponded to an ordered BiBi sequential group transfer mechanism (ordered BiBi) with dead-end inhibition.

Analysis of this scheme suggested that the theoretical reversibility of the catalytic step could be safely ignored, since in our rate studies the total accumulated concentration of product was in the picomolar range and thus negligible. It has been indicated by Cleland (1963) that initial rate studies alone (Johnson and Sutherland, 1973) would result in a family of identical plots for both the RARE BiBi and the ordered BiBi mechanisms, whereas studies of dead-end inhibition would differentiate one from the other. Hence, the general equation of the ordered BiBi mechanism was rearranged and modified to include dead-end ATP^{4-} inhibition and applied to the curves in Fig. 2, as follows:

$$\frac{v}{V_m} = \frac{1}{(K_d/[Mg^{2+}])(1 + K_m\alpha/[MgATP]) + (K_m/[MgATP])(1 + [ATP^{4-}]/K_i) + 1} \tag{3C}$$

where $K_d = [Mg^{2+}]\,[E]/[MgE]$, $K_m = [MgATP]\,[E]/[E\,MgATP]$, $\alpha K_m = [MgE]\,[MgATP]/[MgE \cdot MgATP]$. Since the term $(1 + [ATP^{4-}]/K_i)$ is a constant for the excess 2.5 mM ATP^{4-} curve (Fig. 2), it can be replaced by an arbitrary constant β:

$$\frac{v}{V_m} = \frac{1}{(K_d/[Mg^{2+}]) + (1 + \alpha K_m/[MgATP]) + (\beta K_m/[MgATP]) + 1} \tag{4C}$$

Since the Mg^{2+}/MgATP concentration ratio remains constant (Appendix B), the plotting of the data of Fig. 2 according to rate expression (4C) predicts a second-order rate dependence on substrate concentration. Therefore, the ordered BiBi scheme is not consistent with the kinetic behavior of brain adenylate cyclase (Fig. 2, Table I). The next attempt to fit the data was to use the rate expression for the general RARE BiBi mechanism (Cleland, 1963)

modified to accommodate dead-end inhibition by ATP^{4-}, as follows:

$$\frac{v}{V_m} = \frac{[\text{MgATP}]}{\alpha K_m (1 + K_m/[Mg^{2+}])(1 + [ATP^{4-}]/K_i) + [\text{MgATP}](1 + \alpha K_d/[Mg^{2+}])} \tag{5C}$$

The rate expression simplifies at constant ATP^{4-} and low Mg^{2+} to

$$\frac{V_m}{v} = \alpha K_d \frac{K_m}{[Mg^{2+}]}\left(1 + \frac{[ATP^{4-}]}{K_i}\right) + \frac{[\text{MgATP}]}{[Mg^{2+}]} \tag{6C}$$

Hence, at constant ATP^{4-}, with addition of MgATP, the Mg^{2+}/MgATP concentration ratio remains constant (Appendix B). The last equation simplifies further to

$$\frac{V_m}{v} = \frac{K_{m\,\text{app}}}{[Mg^{2+}]} + Q \quad \text{where} \quad K_{m\,\text{app}} = \alpha K_d K_m\left(1 + \frac{[ATP^{4-}]}{K_i}\right)$$

$$Q = \alpha K_d \frac{[\text{MgATP}]}{[Mg^{2+}]} \tag{7C}$$

Hence, the RARE BiBi mechanism would predict a first-order dependence on Mg^{2+} or MgATP since the concentration of the latter parallels the former (Appendix B), which is consistent with the data of Fig. 2. At high Mg^{2+} and low ATP^{4-} concentrations, the rate expression simplifes to

$$\frac{1}{v} = \frac{\alpha K_m}{V_m [\text{MgATP}]} + \frac{1}{V_m} \tag{8C}$$

Expression (8C) predicts a first-order rate dependence on substrate concen-

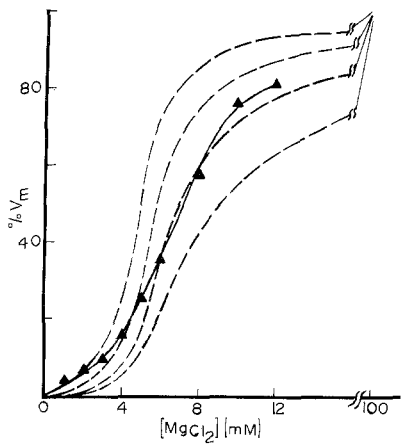

Fig. 10. Comparison of curves generated from the response of adenylate cyclase to $MgCl_2$ based on the RARE BiBi mechanism with an absolute requirement for Me^{2+} activation. The theoretical curves (dashed curve) were plotted using Eq. (5C), the indicated K_d, and the K_m and K_i values listed in Table II. The experimental curve (▲) is a replot of Fig. 4. The predicted and the observed adenylate cyclase activity are plotted as a percentage of V_m.

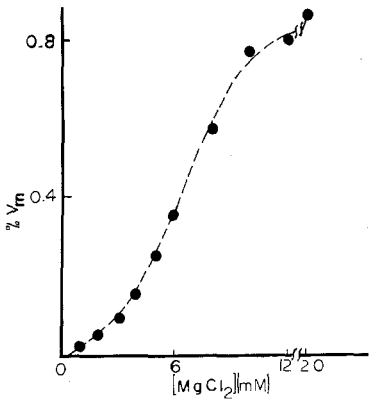

Fig. 11. Theoretical curve based on the RARE BiBi mechanism with Me^{2+} activation not absolutely required. The theoretical curve (dashed curve) is generated using Eq. (9C) and the constants listed in Table II, and by varying the k_0/k ration (basal rate/Me^{2+}-activated rate) and the α values to obtain the best fit. The experimental points (●) are replots of Fig. 4. The values are plotted as a percentage of V_m.

tration at a high and constant concentration of Mg^{2+}, which is consistent with the cooperativity observed in the excess 30 mM Mg^{2+} in the substrate saturation curve (Fig. 1). Figure 10 shows the plots of rate expression (5C) with four different values for K_d (E-Mg) and a curve based on the data of Fig. 4. Figure 10 indicates that rate expression (5C) based on the model requiring Mg^{2+} to form an active enzyme (Walton *et al.*, 1976; Hammes and Rodbell, 1976) does not fit the data of Fig. 4 in two respects: (1) it predicts a value of

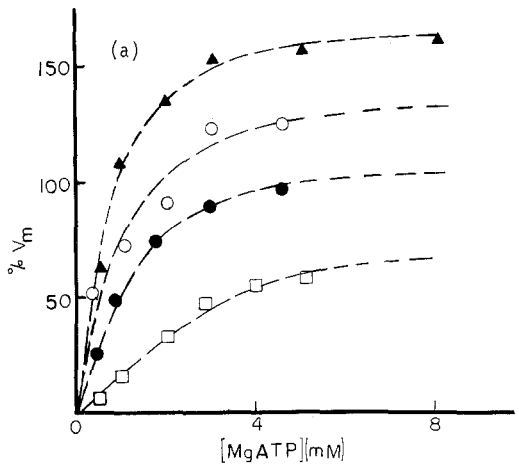

Fig. 12a. Comparison of theoretical substrate saturation curves based on the RARE BiBi mechanism without absolute requirement for Me^{2+} activation. The theoretical curves (dashed curves) were generated as described in the legend to Fig. 11 using the same constants. The experimental points are replots from Figs. 1–3. The activity is plotted as the percentage of V_m for the basal curve for the following conditions: ●, basal; □, +2.5 mM excess ATP; ○, +2.2 mM excess Mg^{2+}; ▲, +30 mM excess Mg^{2+}.

3.5 for $h(MgCl_2)$, whereas the experimental value is 2.6 (Fig. 4) (or $h(Mg_T) = 2.67$ in Table IV); (2) the enzyme is more active at low Mg^{2+} concentration than predicted by rate expression (5C), even when the value of K_d(E-Mg) (Fig. 8 and Table II) is decreased fourfold. The latter was previously observed by De Haen (1974) and led to his conclusion that Mg^{2+} is not an activator of the enzyme. However, both the models requiring obligatory Mg^{2+} activation (Johnson and Sutherland, 1976; Hammes and Rodbell, 1976; Johnson *et al.*, 1979, Garbers and Johnson, 1975) and those without Mg^{2+} activation (De Haen, 1974) failed to predict our experimental observations. Therefore, the model attempted was one that included Mg^{2+} as a modulator but without stipulating that Mg^{2+} in excess of its participation in substrate formation was an obligatory activator for basal activity. This means that the E-MgATP complex can decay directly to form product and enzyme in the absence of Mg^{2+}. The rate expression, as modified from Cleland (Cleland, 1963; King and Altman, 1956) for this mechanism, is as follows:

$$\frac{v}{V_m} = \frac{k_0/k + [Mg^{2+}]/\alpha K_d}{(1 + [Mg^{2+}]/K_d)(1 + [ATP^{4-}]/K_i)(K_m/[MgATP]) + (1 + [Mg^{2+}]/\alpha K_d)} \tag{9C}$$

For high excess of Mg^{2+}, this equation reduces to

$$\frac{v}{V_m} = \frac{\alpha^{-1}}{K_m/[MgATP] + \alpha^{-1}}$$

where α is a constant equal to 1. Thus, for the excess 30 mM Mg^{2+} substrate saturation curve (Fig. 1), the mechanism in rate expression (9C) predicts a first-order rate dependence on substrate concentration. For excess constant

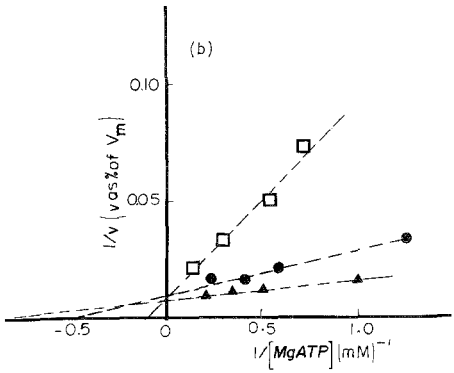

Fig. 12b. Lineweaver–Burk plot.

ATP^{4-} and low Mg^{2+} concentrations, the equation becomes

$$\frac{v}{V_m} = \frac{k_0/k}{K_{m\,app}/[MgATP]} + 1$$

Accordingly, rate expression (9C) is also consistent with the excess 2.5 mM ATP^{4-} in the substrate saturation curve (Fig. 2) showing a first-order rate dependence on MgATP (Table I). Furthermore, Fig. 11 shows a plot of percent v/V_m versus increasing $MgCl_2$ concentration at constant 5 mM ATP_T, where the predicted curve follows closely in shape and slope (with a Hill cooperativity of 2.5) the experimentally observed curve. Hence, since a model requiring obligatory Mg^{2+} activation (Johnson and Sutherland, 1973) predicts a Hill value of 4, we concluded that the observed value of 2.6 for the brain enzyme (Fig. 4 and Table IV) and the fat cell enzyme (Harris *et al.*, 1979) indicates that these enzymes do not have an obligatory Mg^{2+} requirement for basal activity. Figures 12a and 12b show that the theoretical substrate saturation curves and the respective Lineweaver–Burk plots are consistent with the data points obtained from Figs. 1–3. The RARE BiBi mechanism can be further tested by applying it to the effect of $MnCl_2$ on adenylate cyclase activity. As stated previously, Mn^{2+} substitutes for Mg^{2+} in the formation of substrate (Fig. 5) and as an enzyme modulator (Fig. 7). However, the catalytic rates and dissociation constants for Mn^{2+} and MnATP

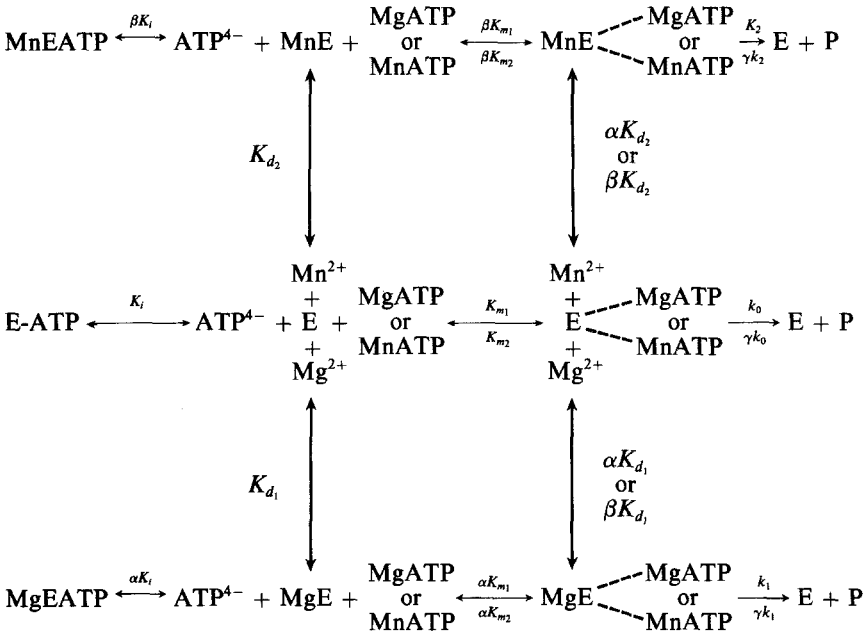

Scheme 1. Equilibria for the RARE BiBi mechanism.

differ from Mg^{2+} and MgATP. The expected interactions are shown in Scheme 1. In Scheme 1 K_{m_1}, K_{m_2}, K_{d_1}, K_{d_2}, and K_i are dissociation constants for MgATP, MnATP, Mg^{2+}, Mn^{2+}, and ATP^{4-} enzyme complexes, α and β are modifying constants following Cleland (Cleland, 1963; King and Altman, 1956), γ is the increase in rate observed with MnATP as the substrate, and k_0, k_1, and k_2 are the relative rates for the E, MgE, and MnE forms of adenylate cyclase. Finally, rate expression (9C) when modified to account for the presence of Mg^{2+} and Mn^{2+} becomes

$$\frac{v}{V_m} = \frac{\left(k_0 + \frac{k_1}{\alpha K_{d_1}}[Mg^{2+}] + \frac{k_2}{\beta K_{d_2}}[Mn^{2+}]\right)\left(\frac{[MgATP]}{K_{m_1}} + \gamma\frac{[MnATP]}{K_{m_2}}\right)}{\left(1 + \frac{[Mg^{2+}]}{K_{d_1}} + \frac{[Mn^{2+}]}{K_{d_2}}\right) + \left(\frac{1 + [Mg^{2+}]}{\alpha K_{d_1}} + \frac{[Mn^{2+}]}{\beta K_{d_2}}\right) \cdot \left(\frac{[ATP^{4-}]}{K_i} + \frac{[MgATP]}{K_{m_1}} + \frac{[MnATP]}{K_{m_2}}\right)} \quad (10C)$$

Rate expression (10C) was used to obtain Fig. 13, a plot of predicted percent v/V_m versus added $MnCl_2$ (0–8 mM) at a constant total 5 mM concentration of ATP and at the indicated concentrations of added $MgCl_2$. Multiple equilibrium equations (1A)–(20A) were used to compute the concentrations of the Me^{2+}, ATP^{4-}, and MeATP complexes, and Table II provided the

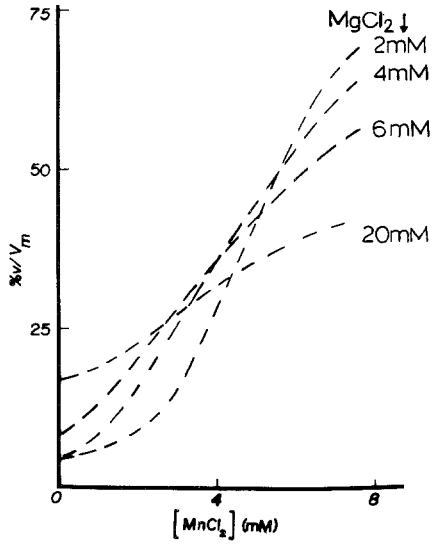

Fig. 13. Theoretical curves based on the RARE BiBi mechanism showing at constant total ATP the response of adenylate cyclase to various $MgCl_2$ concentrations as a function of $MnCl_2$ concentration. These curves were generated using Eq. (10C), the constants listed in Table II, the K_0/k ratio as previously determined (Fig. 11), and by varying the k_2/k_1 ratio and γ (the increase in rate observed with MnATP as the substrate). The rsults are plotted as a percentage of V_m.

respective K_d, K_i, and K_m values required to theoretically reproduce the assay conditions described for Fig. 7a. Comparison of Fig. 7a with Fig. 13 shows that rate expression (10C) predicts the observed kinetic behavior of brain adenylate cyclase in the presence of variable $MgCl_2$ and $MnCl_2$ concentrations (Fig. 7a).

The RARE BiBi mechanism was adapted to account for $CaCl_2$ inhibition of the enzyme which, as previously shown, involves the formation of CaATP, a competitor of the active site. Thus, CaATP is a dead-end inhibitor, much the same as ATP^{4-}. The modified form of Eq. (9C) with the inclusion of CaATP inhibition is as follows:

$$\frac{v}{V_m} = \frac{\frac{k_0}{k} + \frac{[Mg^{2+}]}{\alpha K_{d_1}}}{\left(1 + \frac{[Mg^{2+}]}{K_{d_1}}\right)\left(1 + \frac{[ATP^{4-}]}{K_{i_1}} + \frac{[CaATP]}{K_{i_2}}\right)\frac{K_m}{[MgATP]} + \left(1 + \frac{[Mg^{2+}]}{\alpha K_{d_1}}\right)} \tag{11C}$$

Rate expression (11C) can be used to generate theoretical curves that fit the data of Fig. 9. The applicability of the RARE BiBi mechanism implies group transfer at the active site involving the exchange of PP_i between ATP^{4-} and a pyrophosphate accepting group in the active site, with the eventual formation of cyclic AMP and release of the two products cyclic AMP and PP_i (Scheme 2). Scheme 3 summarizes the RARE BiBi mechanism showing ATP^{4-} and CaATP dead-end inhibition in the same square-shaped skeleton used in the general modifier mechanism of Botts and Morales (1953). The RARE BiBi mechanism is known to show a second-order dependence on substrate concentration unless in a steady-state condition and with a relatively insignificant flux during the precatalytic equilibrium. The first-order dependence observed in Fig. 1 has the special significance of demonstrating that our experimental conditions maintain the reaction in a steady state with insignificant product equilibrium and reversibility. It has been shown (Drummond *et al.*, 1971;

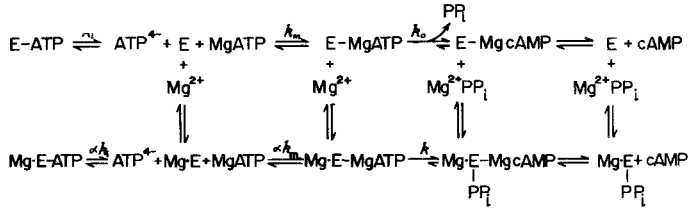

Scheme 2. Random rapid equilibrium BiBi mechanism for rat brain adenylate cylase with Mg^{2+} activation not required.

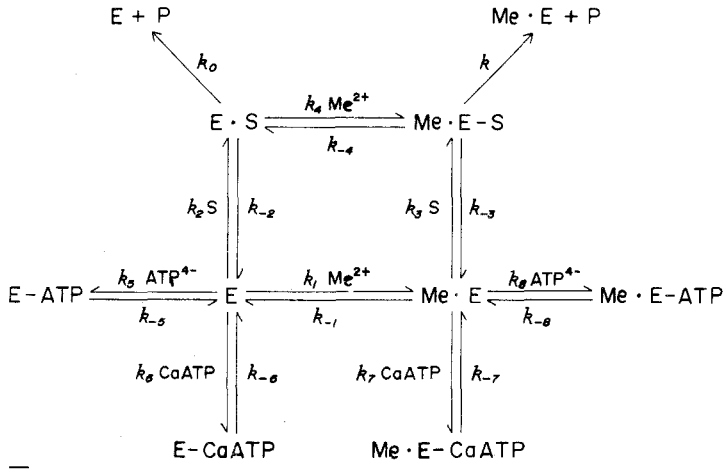

Scheme 3. RARE BiBi mechanism including ATP^{4-} and CaATP dead-end inhibitions as applied to initial rate studies. $Me^{2+} = Mg^{2+}$ or Mn^{2+}.

Johnson and Sutherland, 1973; Harris *et al.*, 1979; Brydon-Golz *et al.*, 1977) that the responsiveness of adenylate cyclase to stimulation by hormones or neurotransmitters is controlled by an obligatory Mg^{2+} requirement that exceeds the one participating in substrate formation. The RARE BiBi mechanism predicts a Hill coefficient of 4 when an absolute requirement for Mg^{2+} is stipulated. Therefore, the RARE BiBi mechanism predicts that hormones will increase $h(MgCl_2)$ from its basal value of 2.6 to values close to 4 (Table IV) because hormones induce an absolute requirement for Mg^{2+}. The finding that CF_1-ATPase requires Mg^{2+} for binding to the membrane and reconstitution of allotopic properties (Bennun and Racker, 1969) suggests a similar obligatory participation of Mg^{2+} in the formation of a hormone receptor-Mg^{2+}–adenylate cyclase complex (Bennun, 1975; Harris and Bennun, 1976). Hormones tend to increase from first to second order the rate dependence on both Mg^{2+} and ATP^{4-} concentrations (Table IV) if ATP^{4-} and adenylate cyclase become competitive ligands for a Mg^{2+} receptor–hormone complex. If the latter proposition for a Mg^{2+}mediated coupling of hormone–receptor complex with adenylate cyclase is included in rate expression (9C), $h(MgCl_2)$ will increase from its basal value of 2.6 to up to 4.6 in the presence of hormones (Harris *et al.*, 1979).

Discussion

Birnbaumer *et al.* (1969) concluded that Mg^{2+} is an allosteric activator of adenylate cyclase in fat cell ghosts. De Haen (1974), using the data of Birnbaumer *et al.* (1969), indicated that it was not necessary to postulate

allosteric activation by Mg^{2+}. This discrepancy is due to the use (Birmbaumer *et al.*, 1969) of lower Mg^{2+} concentrations [K_d(E-Mg) = 3 (Drummond *et al.*, 1971) or 4.7 in Table II] than that required to reach 75% saturation, which is needed to derive useful kinetic information (Deranleau, 1969; Weber, 1965). Garbers and Johnson (1975), using detergent-dispersed preparations of cerebellar and ventricular adenylate cyclase, tested the validity of several models under conditions which maintained the free metal concentrations at essentially constant levels. The kinetics obtained were consistent with a two-reactant sequential mechanism where free cation is an obligatory activator and ATP^{4-} is not a potent inhibitor. However, it has been demonstrated (Johnson *et al.*, 1979) that the detergent-dispersed system does not behave in the same manner as the intact membrane. Furthermore, the concentration range of uncomplexed ATP^{4-} used by Garbers and Johnson (1975) was low and led, therefore, to the loss of kinetic information on the possible inibitory effects of ATP^{4-}. However, since ATP^{4-} shows a K_i equal to one-fourth the K_m for MgATP (Table I), we conclude, contrary to other investigators (Garbers and Johnson, 1975; Rodan *et al.*, 1980a) and in agreement with De Haen (1974), that ATP^{4-} is a potent inhibitor of the active site. The addition of ATP^{4-} decreased the equilibrium concentrations of Mg^{2+} but did not change V_m (Fig. 2b). Thus, we conclude, contrary to Garbers and Johnson (1975), that the equilibrium concentrations of Mg^{2+} associated with equimolar additions of $MgCl_2$ and ATP^{4-} do not activate the enzyme significantly. The data reported in Fig. 1b indicate that the addition of high concentrations of Mg^{2+} is associated with an increase in V_m and a decrease in $K_{m\,app}$, which can be explained by the decrease in the concentration of ATP^{4-}. Lineweaver–Burk plots of adenylate cyclase activity as a function of substrate concentration at different concentrations of Mg^{2+} (Figs. 1b and 3b) show a noncompetitive behavior, indicating that Mg^{2+} interacts with a regulatory site which is distinct from the active site (Birmbaumer *et al.*, 1969). The addition of $CaCl_2$ to the reaction mixtures for the assay of adenylate cyclase is associated with the formation of CaATP as well as the release of Ca^{2+}. Either or both of these species could be inhibitors of adenylate cyclase (Johnson and Sutherland, 1973; Steer *et al.*, 1975; Harris *et al.*, 1979). Figure 9c shows competition between CaATP and the substrate. Hence, contrary to previous proposals (Johnson and Sutherland, 1973; Steer *et al.*, 1975), the $CaCl_2$ inhibition of adenylate cyclase is mostly, if not entirely, due to interaction of CaATP with the active site. However, even though CaATP shows a high affinity for the enzyme (Table I), Mg^{2+} can easily displace Ca^{2+} from ATP and reduce the concentration of CaATP [K_a (MgATP) $= -20 \times 10^3\ M^{-1}$, K_a(CaATP) $= -9 \times 10^3\ M^{-1}$] (Taqui-Khan and Martell, 1962, 1966). The concentration of Mg^{2+} in the intracellular fluid is much higher than that of Ca^{2+} (10^{-3} versus 10^{-6} M) (Veloso *et al.*, 1973) and is practically constant, except for certain pathological states (Seeling, 1980). However, the fractions of divalent metal existing as Mg^{2+} and MgATP, as well as Mn^{2+} and MnATP, may fluctuate

due to changes in the concentrations of metabolic products and intermediates that can complex Mg^{2+} or Mn^{2+} (ATP^{4-}, amino acids, carboxylic acids, and organic phosphates). The cytoplasmic concentration of Ca^{2+} is variable, due not only to the same metabolic effects as those for Mg^{2+} but also to mitochondrial Ca^{2+} export and membrane import (extracellular, 10^{-3} M; mitochondrial, 10^{-2} M) (Rasmussen, 1970; Rasmussen and Goodman, 1975). Accordingly, since the affinity of the enzyme is considerably higher for CaATP than for MgATP, small changes in the concentration of Mg^{2+} could have a stronger activating effect by decreasing CaATP than by any outright increase in MgATP concentration. Table I indicates that the affinity of brain adenylate cyclase for CaATP (K_i = 0.06 mM) is much greater than for ATP^{4-} (K_i = 0.27 mM). Hence, inhibition of brain adenylate cyclase would be maximal if the peaks in the concentrations of ATP^{4-} and Ca^{2+} on the cytoplasmic side of the membrane are synchronized (e.g., early in the action potential during the depolarization phase). Thus, the activity of adenylate cyclase during the neurotransmission cycle may be influenced by synchronization with the operation of ATPase and Ca^{2+} fluxes. This assumption would be consistent with the folowing findings: (1) the activation of adenylate cyclase mediated by the norepinephrine-dependent alpha receptor is believed to promote calcium influx (Rasmussen, 1970) and mobilization of membrane-bound Ca^{2+} (Mitchell *et al.*, 1977) in response to depolarization; (2) the Ca^{2+} concentration in the cytosol is known to play an important role in the intracellular transmission of messages from the alpha adrenergic receptor system (Rasmussen, 1970); (3) norepinephrine, in the brain, activates adenylate cyclase through an alpha receptor (Perkins and Moore, 1973; Schultz and Daly, 1973) coupled to Ca^{2+} release from bound membrane pools, which are thought to be associated either with the inner surface of the plasma membrane (Mitchell *et al.*, 1977) or to be located close to it. Therefore, neurotransmitter-dependent activation of adenylate cyclase may increase endogenous Ca^{2+} which will inhibit ATPase and, therefore, increase the concentrations of ATP^{4-} and CaATP on the cytoplasmic side of the membrane, which would then turn off the activity of the enzyme (Brydon-Golz *et al.*, 1977). Contrary to previous findings (Londos and Preston, 1977) for the liver enzyme, Fig. 5a shows considerable dissimilarities in the V_m of the brain enzyme for MgATP and MnATP. Furthermore, Table I indicates that K_m(MgATP) is 16 times greater than K_m(MnATP). Thus, competition between MgATP, MnATP, ATP^{4-}, and CaATP for the active site of adenylate cyclase shows an order of affinity CaATP > MnATP > ATP^{4-} > MgATP, and an order of activity MnATP > MgATP > CaATP = ATP^{4-} = 0 (Table I). It was also shown that Mn^{2+} and Mg^{2+} compete for the same activating site (Fig. 7). Hence, Mg^{2+} is a weaker activator (Table II), which, in high concentrations, displaces Mn^{2+} from the regulatory site (Table V) and paradoxically reduces the activity of the enzyme (Figs. 7 and 11). Moreover, the increase of V_m observed with Mn^{2+} and Mg^{2+}-dependent activation (Fig.

8) occurs without a change in K_m for either MgATP or MnATP, or $K_i(ATP^{4-})$ (Tables I and II). Furthermore, the inhibitory effect of low concentrations of Ca^{2+} was related to a competitive displacement of Mg^{2+} from the regulatory site without an effect on the relative affinity shown by the active site for either the substrate or ATP^{4-}. Hence, the data in Table II indicate competition for the regulatory site between Mg^{2+}, Mn^{2+}, and Ca^{2+} with an order of affinity $Ca^{2+} > Mn^{2+} > Mg^{2+}$, and an order of activity $Mn^{2+} > Mg^{2+} > Ca^{2+}$.

The data reported in Table II show that the kinetics of adenylate cyclase follows the random rapid equilibrium BiBi group transfer mechanism of Cleland (1963) only when the stipulation that free Mg^{2+} is not required for basal enzyme activity (Figs. 10 and 11) is introduced. Therefore, considering the low affinity of the enzyme for Mg^{2+} (De Haen, 1974; Drummond, *et al.*, 1971) (Table II), its absolute requirement for Mg^{2+} appears to be highly unlikely since its activity is relatively too high when observed in the near absence of excess Mg^{2+} (Fig. 2). Furthermore, the computer-generated curves based on this model (Figs. 12a and 12b) closely correspond with the data from Figs. 1–3, which would also indicate that there is Mg^{2+} activation but that it is not absolutely required for enzyme activity. The applicability of the RARE BiBi model is further confirmed by its ability to predict the complex response of the enzyme at various total concentrations of $MgCl_2$ and $MnCl_2$ (Fig. 13). Furthermore, the model also predicts a change in the Hill cooperativity for the $MgCl_2$ saturation curve (Fig. 4) from a basal value of 2.6 to 4.0 in the presence of norepinephrine (Table IV). This change in h may indicate that excess Mg^{2+} is obligatorily required for the norepinephrine-dependent (Brydon-Golz *et al.*, 1977) or hormone-dependent stimulation of adenylate cyclase (Harris *et al.*, 1979; Harris and Bennun, 1976).

Acknowledgments

The work by H. O. was carried out in partial fulfillment of the requirements for the Ph.D. degree of the Graduate Program of Zoology, Rutgers University; the work of K. B. was in fulfillment of a special project as a medical student in CMDNJ; S. F. is on leave from the Instituto Butantan, Sao Paulo, Brazil. The assistance of Mrs. N. Bennun and Mrs. Rafaela Cruz is gratefully acknowledged. The work was supported by the National Institutes of Health Biomedical Support Grant RR 7059.

References

Bennun, A. (1974). *Ann. N.Y. Acad. Sci.* **227,** 116–145.
Bennun, A. (1975). *BioSystems* **7,** 230–244.
Bennun, A., and Racker, E. (1969). *J. Biol. Chem.* **244,** 1325–1331.

Birnbaumer, L., Pohl, S. L., and Rodbell, M. (1969). *J. Biol. Chem.* **244,** 3468–3476.
Botts, J., and Morales, M. (1953). *Trans. Faraday Soc.* **49,** 696–707.
Brown, B. L., Ekins, R. P., and Albano, J. D. M. (1972). In *Advances in Cyclic Nucleotide Research,* Vol. 2, Raven Press, pp. 25–40.
Brydon-Golz, S., Ohanian, H., and Bennun, A. (1977). *Biochem. J.* **166,** 473–483.
Cleland, W. W. (1963). *Biochim. Biophys. Acta* **67,** 104–137; 173–187.
De Haen, C. (1974). *J. Biol. Chem.* **249,** 2756–2762.
Derenleau, D. A. (1969). *J. Am. Chem. Soc.* **91,** 4044–4054.
Drummond, G. I., and Duncan, L. (1976). *J. Biol. Chem.* **245,** 976–983.
Drummond, G., Severson, D. L., and Duncan, L. (1971). *J. Biol. Chem.* **246,** 4166–4173.
Garbers, D. L. and Johnson, R. A. (1975). *J. Biol. Chem.* **250** 8449–8456.
Gilman, A. G. (1970). *Proc. Natl. Acad. Sci. USA* **67,** 305–312.
Glowinski, J. and Iverson, L. C. (1966). *J. Neurochem.* **13,** 655–669.
Glynn, P., Cooper, D. M. F., and Schulster, D. (1979). *Mol. Cell. Endocrinol.* **13,** 99–121.
Hanski, E., Sevilla, N., and Levitzki, A. (1977). *Eur. J. Biochem.* **76,** 513–520.
Hammes, G. G., and Rodbell, M. (1976). *Proc. Natl. Acad. Sci. USA* **73,** 1189–1192.
Harris, R., Bennun, A. (1976). *Mol. Cell. Biochem.* **13,** 141–146.
Harris, R., Cruz, R., and Bennun, A. (1979). *BioSystems* **11,** 29–46.
Hill, A. V. (1913). *Biochem. J.* **7,** 471–480.
Johnson, R. A., and Sutherland, E. W. (1973). *J. Biol. Chem.* **248,** 5114–5121.
Johnson, R. A., Savr, W., and Jokobs, K. H. (1979). *J. Biol. Chem.* **254,** 1094–1101.
King, E. L., and Altman, C. (1956). *J. Phys. Chem.* **60,** 1375–1381.
Lineweaver, H. and Burk, D. (1934). *J. Am. Chem. Soc.* **56,** 658–666.
Londos, C., and Preston, M. S. (1977). *J. Biol. Chem.* **252,** 5951–5956.
Lowry, O. H., Rosebrough, N. J., Farr, A. L., and Randall, R. J. (1951). *J. Biol. Chem.* **193,** 265–275.
Michell, R. H., Jones, L. M., and Jafferji, S. S. (1977). *Biochem. Soc. Trans.* **5,** 77–81.
Neer, E. J. (1979). *J. Biol. Chem.* **254,** 2089–2096.
Ohanian, H., Borhanian, K., and Bennun, A. (1978). *Biochem. Soc. Trans.* **6,** 1179–1182.
Perkins, J. P. (1973). In *Advances in Cyclic Nucleotide Research,* Vol. 3, Raven Press, New York, pp. 1–61.
Perkins, J. P., and Moore, M. M. (1973). *J. Pharmacol. Exp. Ther.* **185,** 371–378.
Rall, T. W., and Sutherland, E. W. (1958). *J. Biol. Chem.* **232,** 1065–1076.
Rasmussen, H. (1970). *Science* **170,** 404–412.
Rasmussen, H., and Goodman D. B. P. (1975). *Ann. N.Y. Acad. Sci.* **253,** 789–796.
Rodan, S. B., Golub, E. E., Egan, J. J. and Rodan, G. A. (1980a). *Biochem. J.* **185,** 629–637.
Rodan, S. B., Egan, J. J., Golub, E. E., and Rodan, G. A. (1980b). *Biochem. J.* **185,** 617–627.
Rodbell, M., Lin, M. C., Solomon, Y., Londos, C., Harwood, J. P., Mortin, B. R., Rendell, M., and Berman, M. (1975). In *Advances in Cyclic Nucleotide Research,* Vol. 5, Raven Press, New York pp. 3–29.
Schultz, J., and Daly, J. W. (1973). *J. Neurochem.* **21,** 1319–1326.
Seeling, M. S. (1980). In *Magnesium Deficiency in the Pathogenesis of Disease,* Plenum Press, New York.
Severson, D. L., Drummond, G. I. and Sulakhe, P. V. (1972). *J. Biol. Chem.* **247,** 2949–2958.
Steer, M. L., and Levitzki, A. (1975). *J. Biol. Chem.* **250,** 2080–2084.
Steer, M. L., Atlas, D., and Levitzki, A. (1975). *N. Engl. J. Med.* **292,** 409–414.
Sutherland, E. W., Rall, T. W., and Menon, T. (1962). *J. Biol. Chem.* **237,** 1220–1227.
Taqui-Khan, M. M., and Martell, A. E. (1962). *J. Phys. Chem.* **66,** 10–15.
Taqui-Khan, M. M., Martell, A. E. (1966). *J. Am. Chem. Soc.* **88,** 668–671.
Veloso, D., Guynn, R. W., Oskarsson, M., and Veech, R. L. (1973). *J. Biol. Chem.* **248,** 4811–4819.
Walton, K. G., and Baldessarini, R. J. (1976). *J. Neurochem.* **27,** 557–564.
Weber, G. (1965). In *Molecular Biophysics,* B. Pulman and M. Weissbluth, eds., Academic Press, pp. 369–396.

Appendix A. Equilibrium Concentrations of MgATP, ATP^{4-}, and Mg^{2+} Under Experimental Condition Where Excess Mg^{2+} is kept Constant and MgATP is Increased

MgATP (mM) (added)	Mg_T (mM)	ATP_T (mM)	Mg^{2+} (mM)	MgATP (mM) (equilibrium)	ATP^{4-} (mM)
0.1	0.1	0.1	0.0528	0.047	0.0467
0.3	0.3	0.3	0.1070	0.192	0.0945
0.5	0.5	0.5	0.1451	0.354	0.1282
1.0	1.0	1.0	0.2137	0.783	0.1906
2.0	2.0	2.0	0.3159	1.682	0.2793
3.0	3.0	3.0	0.3931	2.660	0.3475
5.0	5.0	5.0	0.5156	4.478	0.4559
8.0	8.0	8.0	0.6595	7.331	0.5833
10.0	10.0	10.0	0.7407	9.247	0.6552
		+ 30 mM excess $MgCl_2$			
0.1	30.1	0.1	30.0	0.996	0.00017
0.3	30.3	0.3	30.0	0.299	0.00052
0.5	30.5	0.5	30.0	0.498	0.00087
1.0	31.0	1.0	30.0	0.996	0.00174
2.0	32.0	2.0	30.0	1.993	0.00348
3.0	33.0	3.0	30.1	2.990	0.00523
5.0	35.0	5.0	30.1	4.983	0.00871
8.0	38.0	8.0	30.2	7.974	0.01394
10.0	40.0	10.0	30.2	9.967	0.01742

Appendix B. Equilibrium Concentrations of MgATP, ATP^{4-}, and Mg^{2+} Under Experimental Conditions Where ATP^{4-} is kept Constant and MgATP is Increased

Mg^{2+} (mM)	ATP^{4-} (mM)	MgATP (mM)	$[MgATP]/[Mg^{2+}]$
0.0058	2.20	0.244	42.1
0.0115	2.22	0.488	42.4
0.0229	2.23	0.976	42.6
0.0343	2.24	1.460	42.9
0.0455	2.25	1.950	43.4
0.0677	2.27	2.930	43.0
0.0896	2.29	3.910	43.4
0.1110	2.31	4.880	43.9
0.1320	2.33	5.860	44.0
0.200	2.33	8.900	44.0

Appendix C. Equilibrium Concentrations of MgATP, ATP^{4-}, and Mg^{2+} Under Experimental Conditions Where Mg^{2+} is kept Constant as MgATP is Increased[a]

Mg^{2+} (mM)	ATP^{4-} (mM)	MgATP (mM)	$[MgATP]/[ATP^{4-}]$
2.210	0.009	0.39	42.10
2.221	0.018	0.78	42.28
2.226	0.023	0.97	42.49
2.045	0.040	1.55	39.80
2.056	0.049	1.94	39.11
2.083	0.073	2.91	39.86
2.135	0.119	4.86	40.84
2.209	0.185	7.78	42.05
2.300	0.267	11.68	43.75
2.091	0.524	20.88	39.85
2.311	0.719	31.65	44.02
2.151	1.020	41.79	40.97

[a] S.E.M. (Mg^{2+}) = 2.169 ± 0.091; S.E.M. ($MgATP/ATP^{4-}$) = 41.42 ± 1.60.

Appendix D. Equilibrium Concentrations of Mg^{2+}, Ca^{2+}, ATP^{4-}, MgATP, and CaATP Under Experimental Conditions Where 0.5 mM Total CaATP is Added and MgATP is Increased

Mg^{2+} (mM)	Ca^{2+} (mM)	ATP^{4-} (mM)	MgATP (mM)	CaATP (mM)
0.0930	0.1666	0.2293	0.406	0.3327
0.1611	0.1478	0.2730	0.378	0.3515
0.2167	0.1348	0.3104	1.280	0.3644
0.2644	0.1249	0.3241	1.730	0.3743
0.3069	0.1171	0.3747	2.190	0.3821
0.4735	0.0931	0.5010	4.520	0.4061
0.7072	0.0712	0.6887	9.280	0.4278